COMPUTATION OF LOAD ON CYLINDRICAL DUCT IN SUPERSONIC FLOW

A project report

Submitted in partial fulfillment of the requirements
for the award of the degrees of

MASTER OF TECHNOLOGY
and
BACHELOR OF TECHNOLOGY

in
AEROSPACE ENGINEERING

by
VINOD K L

under the guidance of
Mr. S. C. Rajan

DEPARTMENT OF AEROSPACE ENGINEERING
INDIAN INSTITUTE OF TECHNOLOGY, MADRAS
CHENNAI - 36
MAY 2004

CERTIFICATE

This is to certify that the project entitled **"Computation of Load on Cylindrical duct in Supersonic flow"**, being submitted by **Vinod K L (AE99039)** in partial fulfillment of the requirements for the award of the degrees of **Master of Technology** and **Bachelor of Technology**, is a bonafide record of work carried out by him at the **Department of Aerospace Engineering, Indian Institute of Technology, Madras**. The contents of this project report have not been submitted and will not be submitted to any other Institute or University for the award of any degree or diploma.

[Mr. S. C. Rajan]
Project Guide
Assistant Professor
Department of Aerospace Engineering

[Prof. Job Kurian]
Head of the Department
Department of Aerospace Engineering

ACKNOWLEDEMENT

I would like to express my heartfelt thanks to my guide **Mr. S. C. Rajan** for being patient and understanding during the course of this work. Working with him has been a great learning experience and I am fortunate to have had him as my guide.

I am indebted to **Dr. P. Sriram** and **Mr. Dhanapal** for providing me with computational resources at the Aero DCF. I would like to thank **Mr. C. S. Sourirajan** for providing me access to the SGI computers in the computer centre. I would also like to thank my friend **L. Krishnamoorthy** for helping me with FLUENT. I would like to express my gratitude to **Prabhu Ramachandran** for his suggestions during this project work.

Last but not the least, I would like to thank my grandmother and mother for their support and encouragement.

Place: Chennai [Vinod K L]

Date:

ABSTRACT

In the present work, supersonic flow past cylindrical duct is studied. Initially, the internal flow through the duct is calculated by distributing supersonic source/sink on the surface. The normal load due to the internal flow is also worked out. As the next step, the entire flow (considering of internal and external flow) past the duct is worked out by distributing vorticity on the boundary. For both cases solution is obtained numerically and the present results obtained are compared with the ones obtained using FLUENT.

Contents

List of Figures

List of Tables

List of Symbols

w	induced velocity at a point
w^*	self induced velocity of the element
q	intensity of source
Q	strength of source
γ	intensity of vorticity (m/s)
Γ	strength of vortex
AR	Aspect ratio of the plate
b	semi-span length of the plate
c	chord length of the plate
a	radius of the cylindrical duct
L	length of the duct
C_N	coefficient of normal force
C_p	coefficient of pressure
M_∞	freestream Mach number
V_∞	freestream velocity
α	angle of attack
μ	Mach cone half angle
β	compressibility factor ($\sqrt{M_\infty^2 - 1}$)
(x, y, z)	cartesian coordinate system
(r, θ, x)	cylindrical coordinate system

Chapter 1

Introduction

The motivation for the present work came from the analysis of the flow field and calculation of load on air-breathing missiles. Prabhu Ramachandran.et.al [9, 10] calculates the normal load on a family of airbreathing configurations. The chosen air-breathing configurations are the ones tested by NASA and AGARD. In the calculations it was assumed that the airbreathing duct is either fully blocked or fully open. The computed values are in reasonable agreement with the measured values. It is interesting that inspite of the geometry being complex and flow field being three dimensional, consideration of the flow field far downstream makes the analysis two dimensional. Main limitation of this method is that the pitching moment cannot be obtained. Inspite of the analysis being subsonic, agreement was found to be good even for supersonic Mach numbers as high as 3 at low angles of attack. This is due to the fact the normal load on the configuration depends only on the cross flow. Even when the Mach number is supersonic, when the angle is small the cross flow Mach number is very small and hence the formalism of incompressible flow could be used. Prabhu Ramachandran.et.al [9], calculates the normal load as well as the pitching moment for the above airbreathing configurations using subsonic panel method.

In the forgoing investigations, inspite of the freestream Mach number being supersonic, the methodology used is for subsonic flow. It should be interesting to find the outcome of calculations, using methods for supersonic flow. As a beginning calculation of the flow and the load on ringwing/cylindrical duct, is taken up. In the Fig. 1.1, the AGARD airbreathing missile configuration is shown. Initially, the presence of the body(missile) is ignored. Only the airbreathing duct is taken up for the analysis. To begin with, the internal flow through the duct is worked out by distributing supersonic sources/sinks on the wall. As the next step, entire flow past the duct is calculated by distributing vorticity on the wall for the supersonic flow.

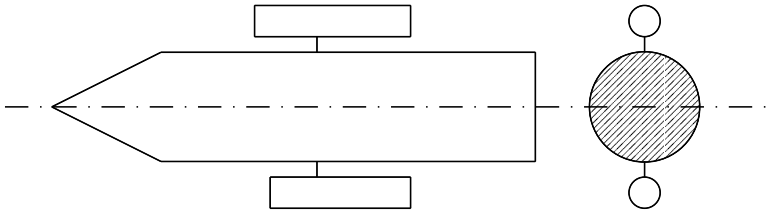

Figure 1.1: AGARD missile configuration

In the recent times, grid wings are being used for the missile. The typical configuration of a grid wing is shown in Fig.1.2 and Fig.1.3. The building block of the grid wing is a square cell. The internal flow through a cell is calculated and at design point operation the total normal load on the grid wing is obtained by adding the contribution of the individual cells. It should be interesting to compare the internal flow in a cylindrical duct and the internal flow in square cells.

It is a known fact that supersonic flows behave differently as compared to their subsonic counterpart. When the flow is inviscid and irrotational, in subsonic flow, the body could be replaced by either a distribution of source/ sink or dipole/vorticicy. The body being solid, the fluid cannot enter it. So the boundary condition to be imposed is that the normal component of velocity on the surface is equal to zero, which is also

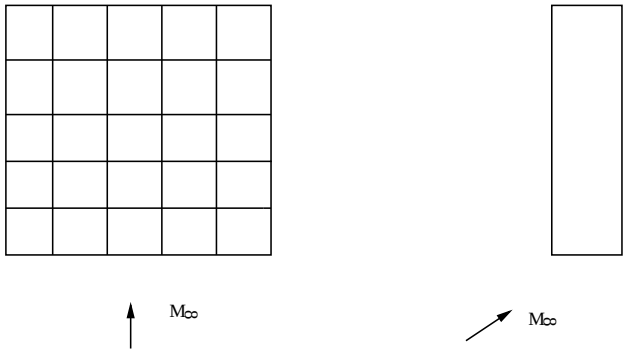

Figure 1.2: Grid wing configuration

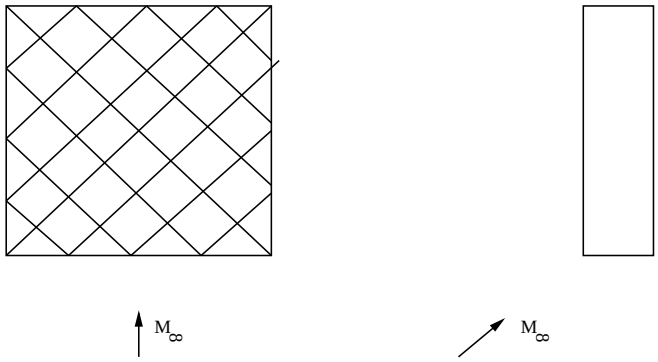

Figure 1.3: Grid wing configuration

known as the no-penetration boundary condition. Imposing this condition, the intensity of the source/sink or vorticity/dipole is determined. The above condition results in an integral equation for the intensity of the singularity. For a body of arbitrary shape, the exact solution of the integral equation is not possible and the equation is solved using panel methods.

The idea of replacing the body by a distribution of singularities is valid even in supersonic flow provided the angle of attack is small. With the above condition fulfilled, the non-linear Euler's equations could be simplified into the linearized equations of supersonic flow. Within the frame work of the linearized theory of supersonic flow, the body could be replaced by distribution of source/sink or dipole/vorticity.

In the present work, distribution of source/sink is used to solve internal flow past circular duct and distribution of vorticity is used to solve actual flow comprising of both internal and external flows past circular duct.

Chapter 2

Mathematical Formulation

2.1 Supersonic Source

2.1.1 Velocity induced by a supersonic source at a point

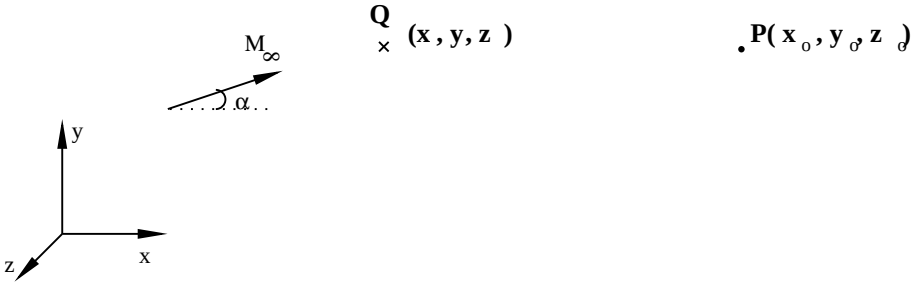

Figure 2.1: Source in supersonic flow

In Fig. 2.1, a source having strength Q in uniform supersonic flow is shown. The angle between the direction of freestream and x axis is α. The source is located at (x,y,z). Potential due to this source at any point $P(x_0,y_0,z_0)$ is given by,

$$\phi = \frac{-Q}{2\pi[(x_0-x)^2-\beta^2\{(y_0-y)^2+(z_0-z)^2\}]^{\frac{1}{2}}} \tag{2.1}$$

which satisfies the following linearized equation for supersonic flow.

$$(1-M_\infty^2)\frac{\partial^2\phi}{\partial x_0^2}+\frac{\partial^2\phi}{\partial y_0^2}+\frac{\partial^2\phi}{\partial z_0^2}=0 \tag{2.2}$$

It should be noted that the expression for potential, Eqn.2.1 is valid only for points (x,y,z) in the downstream Mach cone, such that $x_0 > x$ and

$$(x_0-x)^2-\beta^2\{(y_0-y)^2+(z_0-z)^2\}>0 \tag{2.3}$$

Otherwise potential due to the source is zero.

The velocities induced at point $P(x_0,y_0,z_0)$ are given by

$$u=\frac{\partial\phi}{\partial x_0} \tag{2.4}$$

$$v=\frac{\partial\phi}{\partial y_0} \tag{2.5}$$

$$w=\frac{\partial\phi}{\partial z_0} \tag{2.6}$$

The pressure coefficient according to linear theory of supersonic flow is given by

$$c_p = \frac{-2u}{V_\infty} \tag{2.7}$$

2.1.2 Source distribution on a cylindrical duct

Fig. 2.2, shows a cylindrical duct and the domain of dependance of a point $P(r_0,\theta_0,x_0)$, which lies in the plane $\theta_0=0$. A distribution of source, $q(x,\theta)$ is distributed on the surface of the duct. The shaded region on the surface of the duct is obtained from the intersection of the upstream Mach cone from the point P and the cylindrical duct. In the linear theory the semi-cone angle of the Mach cone is given by $\sin^{-1}\left(\frac{1}{M_\infty}\right)$. Only the source distribution in the shaded region affects the state of flow at P.

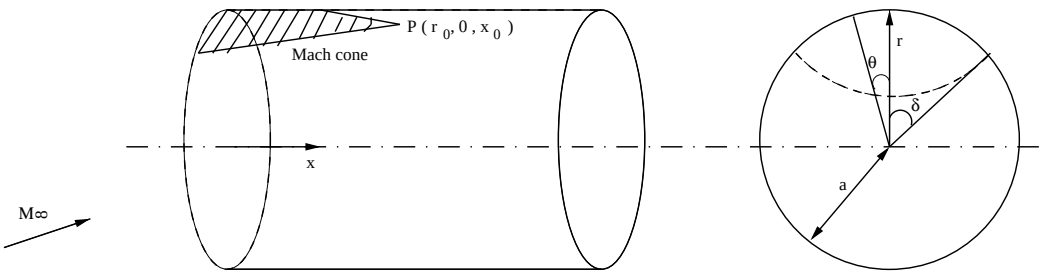

Figure 2.2: Cylindrical duct and upstream Mach cone

The potential, ϕ, at any point (r_0, θ_0, x_0) can be obtained by integrating the distribution of source on the surface of the duct contained in the upstream Mach cone. Nothing that the potential due to a source is given by the Eqn. 2.1, for the present case the expression for potential is given by

$$\phi = -\frac{1}{2\pi}\int_0^{x_0}\int_{\theta_0-\delta}^{\theta_0+\delta}\frac{q(x,\theta)}{\left[(x_0-x)^2-\beta^2(r_0^2+a^2-2ar_0\cos(\theta_0-\theta)\right]^{\frac{1}{2}}}adxd\theta \qquad (2.8)$$

where,

$$\delta = \cos^{-1}\left[\frac{r_0^2+a^2}{2ar}-\frac{(x_0-x)^2}{2ar_0\beta^2}\right] \text{ if } x_0-x \le \beta(a+r_0)$$

$$\delta = \pi \qquad \text{if } x_0-x > \beta(a+r_0)$$

θ and x are shown in the Fig. 2.2.

When the point P lies on the surface of the cylinder, the Eqn. 2.8 simplifies to

$$\phi = -\frac{1}{2\pi}\int_0^{x_0}\int_{\theta_0-\delta}^{\theta_0+\delta}\frac{q(x,\theta)}{\left[(x_0-x)^2-2a^2\beta^2(1-\cos(\theta_0-\theta)\right]^{\frac{1}{2}}}adxd\theta \qquad (2.9)$$

where,

$$\delta = \cos^{-1}\left[1-\frac{(x_0-x)^2}{2a^2\beta^2}\right] \text{ if } x_0-x \le 2a\beta$$

$$\delta = \pi \qquad \text{if } x_0 - x > 2a\beta$$

The governing equation for the strength of source, q is obtained by enforcing the boundary condition that normal velocity at the surface is zero. i.e,

$$\left.\frac{\partial\phi(r_0,\theta_0,x_0)}{\partial r_0}\right|_{r_0=a} + V_\infty \sin(\alpha)\cos(\theta_0) = 0 \tag{2.10}$$

At $\theta_0 = 0$, the governing equation simplifies to

$$\left.\frac{\partial\phi(r_0,0,x_0)}{\partial r_0}\right|_{r_0=a} + V_\infty \sin(\alpha) = 0 \tag{2.11}$$

From Eqn. 2.10 and Eqn. 2.11, it can be seen that

$$\left.\frac{\partial\phi(r_0,\theta_0,x_0)}{\partial r_0}\right|_{r_0=a} = \left.\frac{\partial\phi(r_0,0,x_0)}{\partial r_0}\right|_{r_0=a} \cos(\theta_0) \tag{2.12}$$

On examination of the Eqn. 2.12, a guess is made for that $q(x,\theta)$ to be given as $q(x,0)\cos\theta$. The above assumption is justified below by showing that the Eqn. 2.12 does not get violated under the assumption. Using this assumption and defining $\theta' = \theta_0 - \theta$, Eqn. 2.8, transforms as

$$\phi(r_0,\theta_0,x_0) = -\frac{1}{2\pi}\int_0^{x_0}\int_{-\delta}^{\delta} \frac{q(x,0)\cos(\theta_0-\theta')}{\left[(x_0-x)^2 - \beta(a^2+r_0^2-2ar_0\cos(\theta')\right]^{\frac{1}{2}}} a dx d\theta'$$

Above equation is equivalent to

$$\begin{aligned}\phi(r_0,\theta_0,x_0) &= -\frac{1}{2\pi}\int_0^{x_0}\int_{-\delta}^{\delta} \frac{q(x,0)\cos(\theta_0)\cos(\theta')}{\left[(x_0-x)^2 - \beta^2(a^2+r_0^2-2ar_0\cos(\theta')\right]^{\frac{1}{2}}} a dx d\theta' \\ &- \frac{1}{2\pi}\int_0^{x_0}\int_{-\delta}^{\delta} \frac{q(x,0)\sin(\theta_0)\sin(\theta')}{\left[(x_0-x)^2 - \beta^2(a^2+r_0^2-2ar_0\cos(\theta')\right]^{\frac{1}{2}}} a dx d\theta' \end{aligned} \tag{2.13}$$

Since $\int_{-\delta}^{\delta}\sin\theta'\,d\theta' = 0$ in the second integral in the Eqn. 2.13. Therefore the expression

for $\phi(r_0,\theta_0,x_0)$ reduces to

$$\phi(r_0,\theta_0,x_0) = -\frac{\cos\theta_0}{2\pi}\int_0^{x_0}\int_{-\delta}^{\delta}\frac{q(x,0)}{\left[(x_0-x)^2-\beta^2(a^2+r_0^2-2ar_0\cos(\theta')\right]^{\frac{1}{2}}}\,adxd\theta' \tag{2.14}$$

When $\theta_0 = 0$ is subsituted in Eqn. 2.14,

$$\phi(r_0,0,x_0) = -\frac{1}{2\pi}\int_0^{x_0}\int_{-\delta}^{\delta}\frac{q(x,0)}{\left[(x_0-x)^2-\beta^2(a^2+r_0^2-2ar_0\cos(\theta')\right]^{\frac{1}{2}}}\,adxd\theta' \tag{2.15}$$

Hence,

$$\phi(r_0,\theta_0,x_0) = \phi(r_0,0,x_0)\cos(\theta_0) \tag{2.16}$$

Taking partial derivative of the Eqn. 2.16 with respect to r_0, the following is obtained

$$\frac{\partial\phi(r_0,\theta_0,x_0)}{\partial r_0} = \frac{\partial\phi(r_0,0,x_0)}{\partial r_0}\cos(\theta_0) \tag{2.17}$$

Hence at $r_0 = a$, Eqn. 2.12 is obtained. This shows that the assumption that $q(\theta,x)$ equals to $q(0,x)\cos\theta$ does not violate the governing equation. Hence the assumption that $q(x,\theta_0)$ equals $q(x,0)\cos(\theta_0)$ is justified.

2.2 Supersonic Vortex

2.2.1 Velocity induced by horseshoe vortex element at a point

In Fig. 2.3, the horseshoe element having span length (y_2-y_1) is shown. The expression for the velocity induced by the horseshoe vortex at the point $P(x,y,z)$ is given by Robinson [1] and Ward [7]. In supersonic flow, when vorticity distribution is used an additional difficulty is encountered. The induced velocity becomes infinite and finite part is extracted. The idea is known as Hadamard's finite part. The idea is clearly ex-

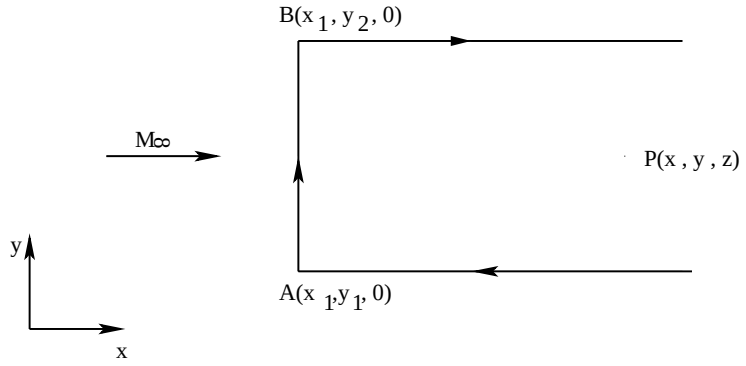

Figure 2.3: Horseshoe element in supersonic flow

plained in Ward [7]. It is also presented in Appendix B. The idea of a finite part of the integral for a general case is given by Robinson [1].

Consider the horseshoe vortex of strength Γ, as shown in Fig. 2.3. Let Ψ be a vector function such that $\Psi = (\psi_1, \psi_2, 0)$, where ψ_1 and ψ_2 are given Eqn. 2.18 and Eqn. 2.19.

$$\psi_1 = \frac{\Gamma}{2\pi}\left[cosh^{-1}\frac{x-x_1}{\beta\sqrt{(y-y_1)^2+z^2}} - cosh^{-1}\frac{x-x_1}{\beta\sqrt{(y-y_2)^2+z^2}}\right] \tag{2.18}$$

and the $cosh^{-1}()$ is to be replaced by 0 when the argument is less than 1, and

$$\psi_2 = -\frac{\Gamma}{2\pi\beta}\left[sin^{-1}\frac{\beta(y-y_1)}{\sqrt{(x-x_1)^2-\beta^2z^2}} - sin^{-1}\frac{\beta(y-y_2)}{\sqrt{(x-x_1)^2-\beta^2z^2}}\right] \tag{2.19}$$

where $sin^{-1}()$ is to be replaced by $\frac{\pi}{2}$ or $-\frac{\pi}{2}$ when their arguments are greater than 1, or smaller than -1, respectively. Also Eqn. 2.18 and Eqn. 2.19 hold only for $x > x_1$ while for $x < x_1$, $\psi_1 = \psi_2 = 0$, because it lies outside the Mach cone.

The hyperbolic curl of a vector Ψ is defined as

$$\nabla_h \times \Psi = \left(\frac{\partial \Psi_z}{\partial y} - \frac{\partial \Psi_y}{\partial z}\right)\hat{i} + \left(\frac{\partial \Psi_x}{\partial z} + \beta^2 \frac{\partial \Psi_z}{\partial x}\right)\hat{j} - \left(\beta^2 \frac{\partial \Psi_y}{\partial x} + \frac{\partial \Psi_x}{\partial y}\right)\hat{k} \qquad (2.20)$$

Now the components of the velocity induced by this horseshoe vortex at a point (x,y,z) is obtained by taking the hyperbolic curl of $\Psi = (\psi_1, \psi_2, 0)$.

$$\begin{aligned} u &= \frac{\Gamma\beta^2}{2\pi}\left[\frac{(y-y_2)z}{[(x-x_1)^2-\beta^2z^2]\{(x-x_1)^2-\beta^2[(y-y_2)^2+z^2]\}^{\frac{1}{2}}}\right. \\ &\quad \left. -\frac{(y-y_1)z}{[(x-x_1)^2-\beta^2z^2]\{(x-x_1)^2-\beta^2[(y-y_1)^2+z^2]]\}^{\frac{1}{2}}}\right] \qquad (2.21) \\ v &= \frac{\Gamma}{2\pi}\left[\frac{(x-x_1)z}{[(y-y_2)^2+z^2]\{(x-x_1)^2-\beta^2[(y-y_2)^2+z^2]\}^{\frac{1}{2}}}\right. \\ &\quad \left. -\frac{(x-x_1)z}{[(y-y_1)^2+z^2]\{(x-x_1)^2-\beta^2[(y-y_1)^2+z^2]\}^{\frac{1}{2}}}\right] \qquad (2.22) \\ w &= \frac{\Gamma}{2\pi}\left[\frac{(x-x_1)(y-y_2)\{(x-x_1)^2-\beta^2[(y-y_2)^2+2z^2]\}}{[(x-x_1)^2-\beta^2z^2][(y-y_2)^2+z^2]\{(x-x_1)^2-\beta^2[(y-y_2)^2+z^2]\}^{\frac{1}{2}}}\right. \\ &\quad - \left.\frac{(x-x_1)(y-y_1)\{(x-x_1)^2-\beta^2[(y-y_1)^2+2z^2]\}}{[(x-x_1)^2-\beta^2z^2][(y-y_1)^2+z^2]\{(x-x_1)^2-\beta^2[(y-y_1)^2+z^2]\}^{\frac{1}{2}}}\right] \qquad (2.23) \end{aligned}$$

It is important to note that the above equations are valid only when

$$(x-x_1)^2 - \beta^2\{(y-y_1)^2+z^2\} > 0$$

For points located in the plane $z = 0$, the components u and v of the induced velocity vanish and the expression for the induced velocity reduces to

$$w = \frac{\Gamma}{2\pi}\left(\frac{\left[(x-x_1)^2-\beta^2(y-y_2)^2\right]^{\frac{1}{2}}}{(x-x_1)(y-y_2)} - \frac{\left[(x-x_1)^2-\beta^2(y-y_1)^2\right]^{\frac{1}{2}}}{(x-x_1)(y-y_1)}\right) \tag{2.24}$$

The equation is valid when

$$(x-x_1)^2-\beta^2(y-y_1)^2 > 0$$

2.2.2 Pressure coefficient

In linearized theory of supersonic flow, coefficient of pressure is given as

$$c_p = -\frac{2u}{V_\infty} \tag{2.25}$$

Since the variables involved in Stokes' theorem are kinematical in nature, the following facts hold good.

If u_l is the velocity along the direction x in the lower part of the panel and u_u is the velocity along the direction x in the upper part of the panel.

$$\gamma = u_u - u_l \tag{2.26}$$

In the above equation γ is the span-wise component of the intensity of vorticity. Specializing Eqn. 2.25 for the points above and below the panel, we obtain,

$$C_{pu} = -\frac{2u_u}{V_\infty} \tag{2.27}$$

$$C_{pl} = -\frac{2u_l}{V_\infty} \tag{2.28}$$

$$\begin{aligned} \Delta C_p &= C_{pl} - C_{pu} \\ &= \frac{2(u_u - u_l)}{V_\infty} \end{aligned} \tag{2.29}$$

From Eqn. 2.26 it follows that

$$\Delta C_p = \frac{2\gamma}{V_\infty} \tag{2.30}$$

Chapter 3

Computational Details

3.1 Supersonic Source panel method

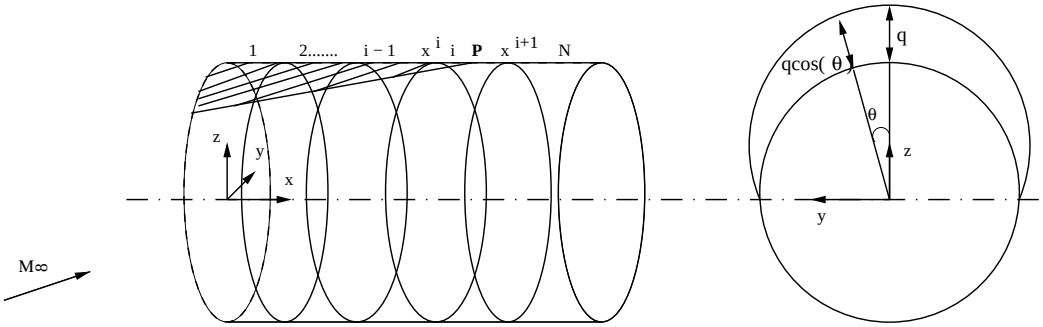

Figure 3.1: Distribution of source panels on cylindrical duct

As shown in the Fig. 3.1. the duct is divided into N number of sub-cylinders. As it is, the intensity of source, q is a function of axial coordinate x and the circumferential coordinate θ. In the previous chapter it is shown that at any station x, the intensity of source, q at an angle θ can be taken as $\cos(\theta)$ times the intensity at $\theta = 0$.

Hence, there is no need to introduce panels along the circumferential direction.In the numerical solution, it is assumed that the intensity is constant over the length of sub-

cylinder. Since the dependance of q on θ is known, the intensity of source distribution on the cylinder is obtained by enforcing the no-penetration conditon only at $\theta = 0$. The no-penetration condition at the plane $\theta = 0$ is given by

$$w^* + w + V_\infty \alpha = 0 \tag{3.1}$$

where w^* is the self induced normal velocity and w is the normal velocity contribution due to the rest of the panels. It is obvious that in Eqn. 3.1, both w and w^* depend on intensity of source.

As mentioned earlier, along the length of panel, intensity is assumed to be constant. Then, q_i is the intensity of the source of the i^{th} panel at $\theta = 0$. Intensity of source, q_1 for the leading panel is first worked out. Being supersonic flow, the intensity q_1 does not depend upon the following panels q_2, q_3..... The values of q_2, q_3... are determined in succession.

Considering the i^{th} panel, the contribution to potential at the control point P comes only from the shaded region shown in Fig. 3.1, which is the domain of dependance of point P. The computation of contribution to normal velocity due to panels $1, 2 \ldots (i-1)$, w_i on i^{th} panel is listed below.

As shown in Fig. 3.1, the j^{th} panel stretches axially from x^j to x^{j+1}. The potential, ϕ_{ji} due to j^{th} panel on i^{th} panel can be obtained by simplifying Eqn. 2.15 and is given by

$$\phi_{ji} = -\frac{q_j}{2\pi} \int_{x^j}^{x^{j+1}} \int_{-\delta}^{\delta} \frac{1}{\left[(x-x_i)^2 - 2a^2\beta^2(1-\cos(\theta)\right]^{\frac{1}{2}}} a dx d\theta \tag{3.2}$$

where δ is given by

$$\delta = \cos^{-1}\left[1 - \frac{(x_i - x_j)^2}{2a^2\beta^2}\right] \text{ if } x_i - x_j \leq 2a\beta$$

$$\delta = \pi \qquad \text{if } x_i - x_j > 2a\beta$$

where x_j is given by $(x^j + x^{j+1})/2$ and x_i is given by $(x^i + x^{i+1})/2$.

The integration in the Eqn. 3.2 is solved numerically using Simpson's rule. Total value of potential, ϕ_i due to other panels at panel i is obtained by summing up the potentials due to all other panels. i.e,

$$\phi_i = \sum_{j=1}^{i-1} \phi_{ji} \tag{3.3}$$

Similarly, $\phi(a+dr,0,x_i)$ and $\phi(a-dr,0,x_i)$ are calculated using the general equation, Eqn. 2.8. w_i is obtained using the equation

$$w_i = \frac{\partial \phi_i}{\partial r} \tag{3.4}$$

The derivative is obtained numerically central difference scheme which is given by

$$\frac{\partial \phi_i}{\partial r} = \frac{\phi(a+dr,0,x_i) - \phi(a-dr,0,x_i)}{2dr} \tag{3.5}$$

During the above calculations for the value of the potential at location i, the contribution of the i^{th} panel is not taken into account.

Self induced velocity is obtained as follows. Since the distribution of source only in the upstream Mach cone contributes to the potential at the control point of i^{th} panel, that the intersection of Mach cone and duct is curved is ignored. Hence the domain of dependance for the calculation of potential at point P is assumed to be flat. It can be shown that

$$w_i^* = -\frac{q_i}{2} \tag{3.6}$$

Details are worked out in the Appendix. A.

The contribution of panels 1 to $(i-1)$ to the normal velocity is given by Eqn. 3.4 is a known quantity. Hence substituting the known value of from w_i Eqn. 3.4 and expression for w_i^* in Eqn. 3.1, the value q_i can be obtained. As mentioned earlier, the intensity of source at any angle θ is given by $q_i \cos(\theta)$.

The total value of potential, ϕ_{it} at the panel i is calculated by adding the self contribution of the i^{th} panel to the ϕ_i given in Eqn.3.3. We then have

$$\phi_{it} = \phi_i - \frac{q_i dx}{4\beta} \tag{3.7}$$

where dx is the axial length of the panel.

The x component of velocity, u_i at the panel i is calculated using Eqn. 2.4. The differentiation is carried out numerically using central difference for the inner panels and one-sided difference for the end-panels. The resulting equations are given by

$$\begin{aligned} u_1 &= \frac{\phi_{2t} - \phi_{1t}}{dx} \\ u_i &= \frac{\phi_{(i+1)t} - \phi_{(i-1)t}}{2dx} \\ u_N &= \frac{\phi_{Nt} - \phi_{(N-1)t}}{dx} \end{aligned} \tag{3.8}$$

The pressure coeffient is calculated using Eqn. 2.25. Now the normal force coefficient is given by

$$C_N = \frac{\sum_{i=1}^{N} \left(\int_0^{2\pi} c_p \cos(\theta) a \, d\theta \right) \Delta x}{\pi a^2} \tag{3.9}$$

where a is the radius of the cylinder. Reference area is based on the cross sectional area of the cylinder.

3.2 Supersonic Vortex panel method

3.2.1 Cylindrical duct

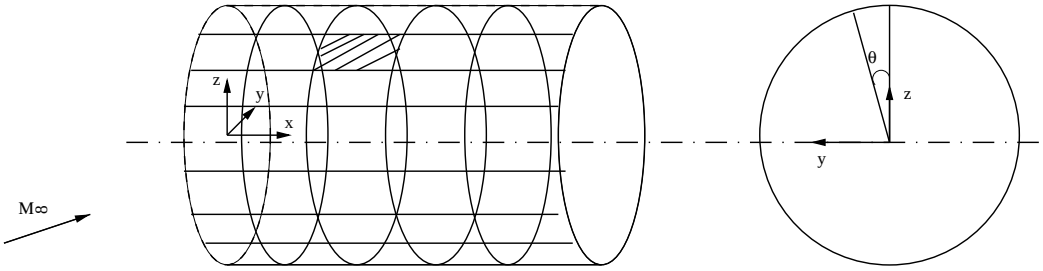

Figure 3.2: Distribution of panels on the cylindrical duct

As the next step the total force on the cylindrical duct/ringwing due to both internal and external flow is worked out by distributing vorticity on the wall of the duct. In the numerical method the duct is divided into number of panels both along circumferential and axial directions.

The choice of vorticity is due to the fact that the velocity just inside and outside the wall of the duct are not same indicating that it would be appropriate to distribute vorticity for modelling the flow. Hence the panel is replaced by a supersonic horseshoe vortex element. The control point is defined as the point where the no-penetration condition for the velocity is imposed. The field points are the points which contribute to the induced velocity at the control point. At a given control point, the induced velocity is a function of two factors. One is the strength of the vortex and the other is the location of the field points. The flow must be tangent to the boundary wall of the duct and the condition is given by

$$w^* + w + V_\infty \alpha \cos(\theta) = 0 \tag{3.10}$$

where as shown in Fig. 3.2, θ is angle which the radial line to the centroid of the panel makes with the z axis. w^* is the self induced velocity of a panel and w is the velocity induced due to other panels.

In the equation given above, w is calculated considering the panels lying in upstream Mach cone of the i^{th} panel. Suppose a panel lies partially in the upstream Mach cone, the partial influence of it is considered. The flow being supersonic, the intensity of vorticity for the panels along the duct entry does not depend on the intensity of vorticity of panels in the downstream. Hence the intensity of vorticity for panels along the duct entry is worked out first and the solution procedure is proceeded towards the duct exit. Let (x_i, y_i, z_i) be the coordinates of the control point lying in the plane $\theta = \theta_i$. Similarly, let (x_j, y_j, z_j) and $\theta = \theta_j$ be respectively be the coordinates and the plane of the panel lying in the upstream Mach cone. To calculate the the induced velocity of j^{th} panel, the following transformation is carried out.

$$\begin{aligned}
x_i' &= x_i \\
y_i' &= y_i \cos(\theta_j) - z_i \sin(\theta_j) \\
z_i' &= (y_i - y_j)\sin(\theta_j) + (z_i - z_j)\sin(\theta_j) \\
x_j' &= x_j \\
y_j' &= y_j \cos(\theta_j) - z_j \sin(\theta_j) \\
z_j' &= 0
\end{aligned} \tag{3.11}$$

The equations 2.22 and 2.23 are used to obtain v_j' and w_j' with respect to the transformed coordinates. The actual normal velocity, w_j induced due to j^{th} panel is obtained

as

$$w_j = w'_j \cos(\theta_i - \theta_j) - v'_j \sin(\theta_i - \theta_j) \tag{3.12}$$

The total value of induced velocity is obtained by summing up the induced velocities of all panels lying within the upstream Mach cone of the i^{th} panel. i.e,

$$w = \sum_j w_j \tag{3.13}$$

The self induced velocity, w^* of the panel on itself is obtained by replacing concentrated bound vortices by distribution of vorticity. The expression for self induced velocity is given by Eqn. 3.14. Detailed derivation of this is given in Appendix. C

$$w^* = -\frac{\gamma\beta}{2} \tag{3.14}$$

Since the values of intensity of panels upstream of the i^{th} (panel under consideration) are known, only the intensity of of vorticity of panel under consideration is unknown. Eqn. 3.10 is solved for the value of intensity of the i^{th} panel. The strength of the horseshoe panel, Γ is given by

$$\Gamma = \gamma \Delta x \tag{3.15}$$

where is Δx is the span length of the panel.

From Eqn. 3.10, Eqn. 3.14 and Eqn. 3.15

$$\Gamma = \frac{2\Delta x(V_\infty \alpha \cos\theta + w)}{\beta} \tag{3.16}$$

In the actual computation, the simplification due to similarity existing in the circumferential direction for the intensity of vorticity, γ is not enforced that $\gamma(x,\theta)$ equals to $\gamma(x,0)\cos\theta$ naturally comes out. The jump in the pressure coefficient across the duct

wall is calculated using the Eqn. 2.30. The coefficient of normal force is calculated using

$$C_N = \frac{\sum\sum(\Delta c_p \cos(\theta)\Delta x a \Delta\theta)}{\pi a^2} \tag{3.17}$$

where a is the radius of the cylinder and $a\Delta\theta$ is the span length of the panel.

3.2.2 Flat Plate

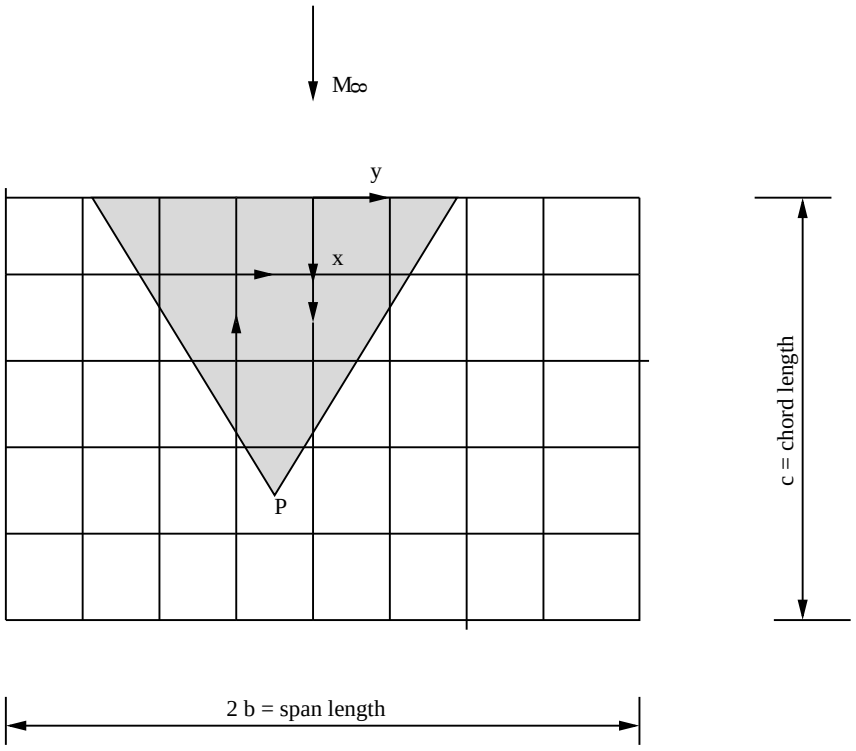

Figure 3.3: Distribution of panels for a finite aspect ratio flat plate

The validation of the method is carried out considering, the case of supersonic flow past finite aspect ratio flat plates. Hence the details of the formalism are briefly explained for also this case. The induced normal velocity due to a horseshoe vortex given by Eqn. 2.24 and Eqn. 3.14 for the self induced velocity are used at each control point.

The flow must be tangent to the surface of the plate and the condition is given by

$$w + w^* + V_\infty \alpha = 0 \tag{3.18}$$

where w^* is the self induced velocity of a panel and w is the velocity induced due to other panels.

In Fig. 3.3, the vortex system contained in the upstream Mach cone of point P is shown. P is the centroid of the panel chosen as a control point. While calculating the induced velocity at P, only those panels lying within the upstream Mach cone(shown shaded in Fig. 3.3) is taken into account. If only part of the panel lies within the Mach cone, partial influence of the panel is worked out. The other panels which are not shaded do not influence the point P. The number of panels is chosen to be large so that the error is minimum.

Initially, the intensity of vorticity for the panels along the leading edge is worked out and proceeded towards the trailing edge. For an interior panel lying between the leading and trailing edges of the plate, the unknown would be only the intensity of vorticity of the panel consideration, since the values of intensity of panels upstream of it are known. Eqn. 3.18 is used to solve the unknown value of intensity. The strength of the horseshoe is given by Eqn. 3.15.

In the actual computation, the simplification due to the symmetry of the body shapes is not used. The boundary condition is satified at all points and symmetry of circulation distribution about the mid-span location naturally emerged.

Knowing the values of γ, the jump in the pressure coefficient is calculated from the Eqn. 2.30. The coefficient of normal load is calculated using

$$C_N = \frac{\sum\sum(\Delta c_p \Delta x \Delta y)}{S} \tag{3.19}$$

where S is the planform area of the plate.

Chapter 4

Results and Discussion

4.1 Internal flow through cylindrical duct

To begin with, the internal flow through the cylindrical duct is worked out by distributing supersonic source on the wall. The radius of the duct is chosen as 1. Results were obtained for different values of length. Angle of attack is varied from 2^o to 10^o. The present results are compared with the ones obtained from FLUENT.

In Fig. 4.1, the variation of the coefficient of normal force C_N versus length of cylindrical strips/panels is shown using different number of panels used for computation. The angle of attack,α, is fixed at 2^o. It can be seen that the results converge with the increase in total number of panels.

In Fig. 4.2, the variation of intensity of source distribution, q, with length of the duct is shown. It can be seen that it is oscillatory. It can also be seen that the amplitute of the oscilation decreases with length. The behaviour of intensity of source versus length for the present case of supersonic flow is not like subsonic flow and hence it is counter-intuitive.

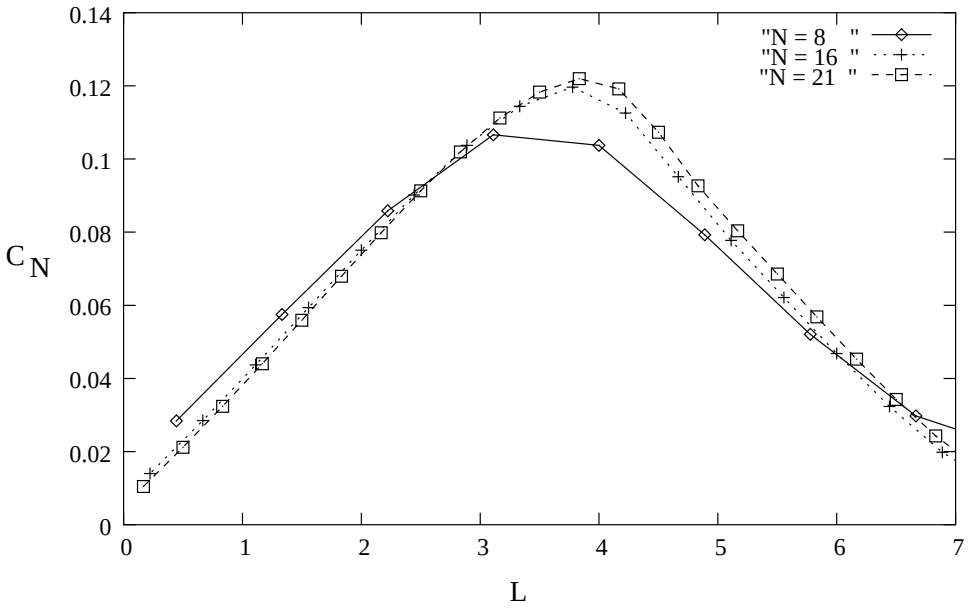

Figure 4.1: Variation of normal force coefficient with length of the duct for different number of cylindrical strips. $M_\infty = 2.5$, $\alpha = 2^o$

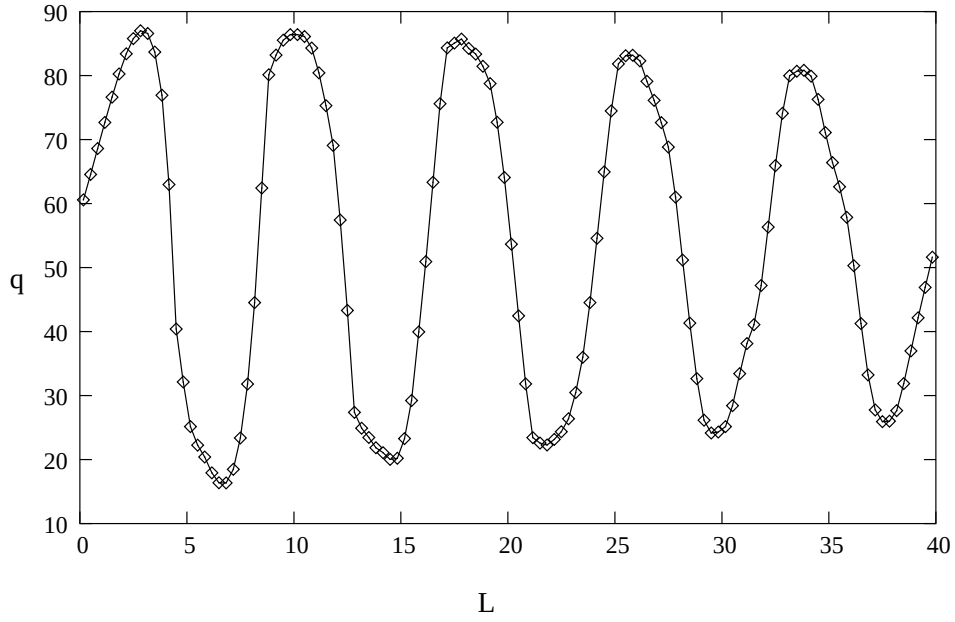

Figure 4.2: Variation of intensity of source at $\theta = 0$ plane along the length of the duct. $M_\infty = 2.5$, $\alpha = 2^o$

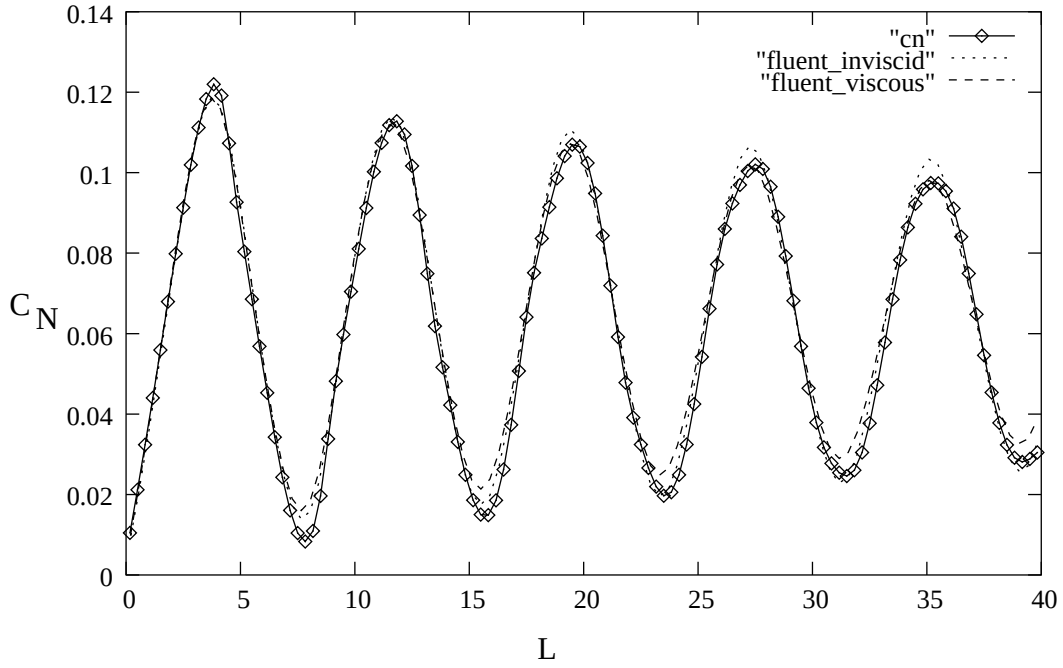

Figure 4.3: Variation of normal force coefficient with length of the duct. $M_\infty = 2.5$, $\alpha = 2^o$. Calculated values are compared with results from FLUENT

In Fig. 4.3, the variation of coefficient of normal force, C_N, with length of the duct is shown. It can be seen that it is oscillatory. It can also be seen that the amplitute of the oscilation decreases with length. The result obtained is compared to one obtained from FLUENT. Results using FLUENT was obtained both for for both inviscid and viscous case. The agreement between the present results and ones obtained from FLUENT is seen to be very good.

In order to solve in FLUENT, the grid was generated in GAMBIT using Cooper's scheme. The radius and the length of the duct were respectively chosen as 5 and 40. The grid spacing was chosen as 0.5. This generated 81 grid points along the length and 64 points along the circumference resulting in total number of grid points on the circumference of the duct being 5184. Later the radius of the duct was scaled down to

1. While specifying the boundary conditions, the inlet was specified as pressure inlet and outlet as pressure outlet. While solving, the conservative Euler equation was solved using second upwinding scheme, which is an implicit scheme. The convergence criteria was given as 10^{-6}.

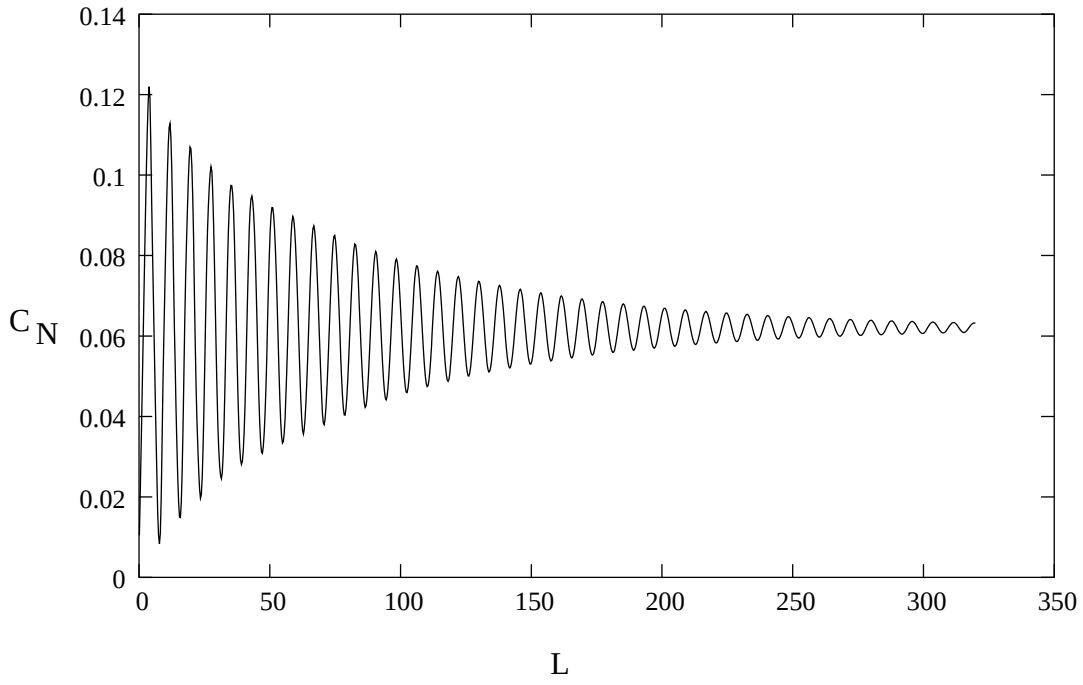

Figure 4.4: Variation of normal force coefficient with the length of the duct. $M_\infty = 2.5$, $\alpha = 2^o$

In Fig. 4.4, the variation of coefficient of normal force, C_N, with length of the duct for values of length sufficiently large is shown. It can be seen that as length increases, the oscillation dies down. As the length is increased indefinitely, C_N tends to a limiting value.

In Fig. 4.5, the variation of coefficient of normal force, C_N, with length of the duct for $\alpha = 5^o$ is shown. It can be seen that the agreement is good upto a value of length around 15. The diameter being 2, slenderness ratio is 7.5. However the agreement is not good at crests and troughs and it is better at crests than at troughs.

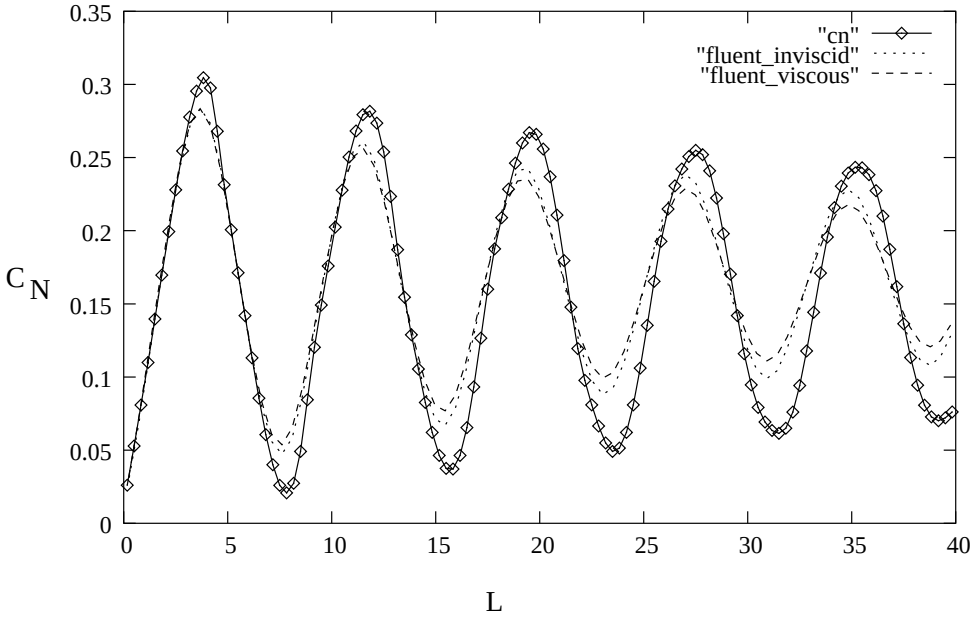

Figure 4.5: Variation of normal force coefficient with the length of the duct. $M_\infty = 2.5$, $\alpha = 5^o$. Calculated values are compared with results from FLUENT

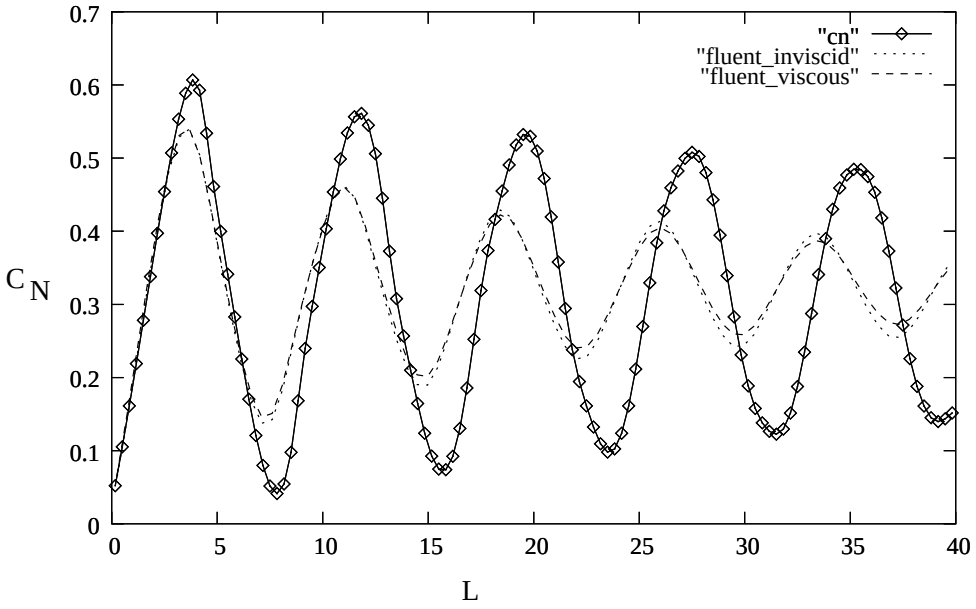

Figure 4.6: Variation of normal force coefficient with the length of the duct. $M_\infty = 2.5$, $\alpha = 10^o$. Calculated values are compared with results from FLUENT

In Fig. 4.6, the variation of coefficient of normal force, C_N, with length of the duct for $\alpha = 10^o$ is shown. It can be seen that the results obtained using FLUENT and the current results start deviating significantly beyond the value of 7(slenderness ratio equals 3.5). Inspite of the deviations the oscillations die and the limiting value obtained using present case andthe extrapolated mean value obtained using FLUENT are nearly same and is given 0.314. It is to be mentioned that when the cross sectional shape of the duct is square, as the length of the duct is increased the oscillations exhibited by normal force coeffiecient persists indefinitely as given in Santhakumar.et.al. [11].

4.2 Flow past rectangular flat plates

In this section, flat plate wings having rectangular planforms exposed in supersonic flow are chosen for the validation. The flow field is calculated using supersonic vortex lattice method. Results were obtained for different aspect ratio of the wing. The calculated value of normal force coefficient is compared with the ones available in literature.

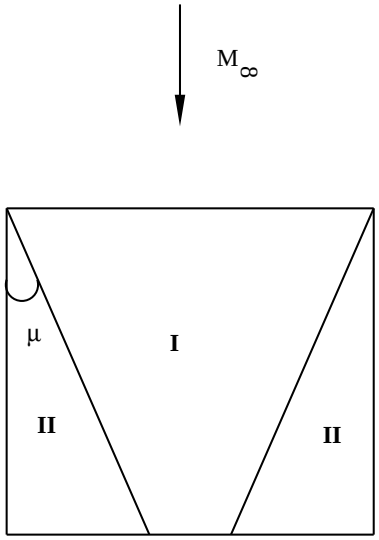

Figure 4.7: Rectangular flat plate wing. $M_\infty = 2.5$, $AR = 1.0$

In Fig. 4.7, the rectangular flat plate having $AR = 1$ in i supersonic free stream Mach number of which is 2.5 is shown. In the interior region I, the flow is two dimensional and in region II, the flow is conical with respect to the end points of the leading edge, in the sense that along a radial line emanating from the intersection of the leading and side edges, the flow variables do not change. In Fig. 4.7, the regions I and II are separated by Mach lines.

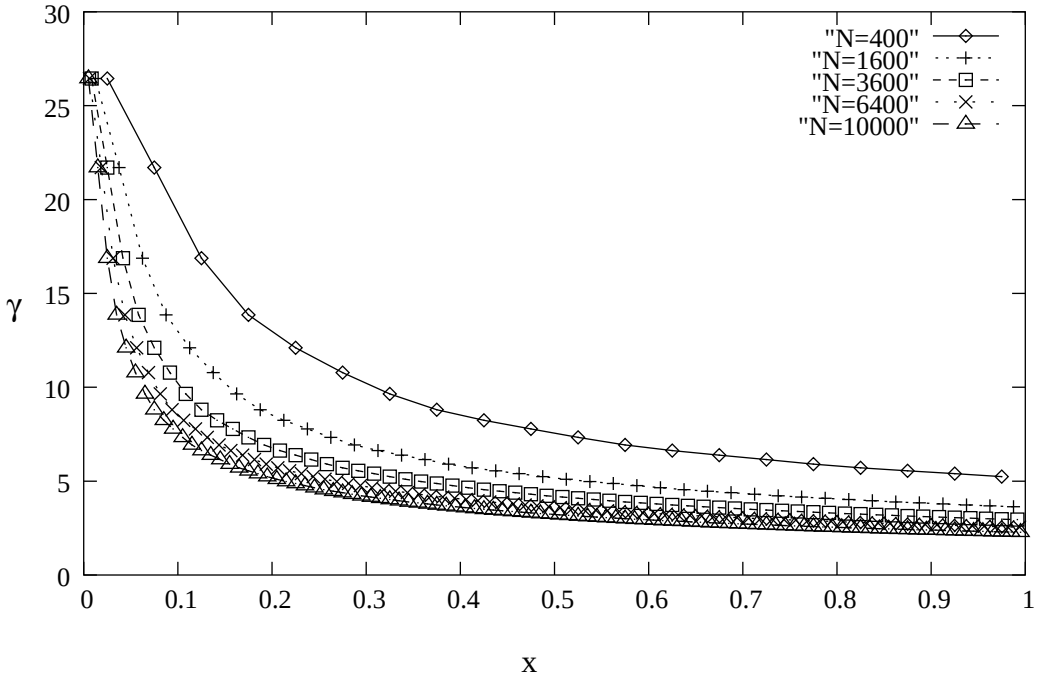

Figure 4.8: Variation of intensity of vorticity along the chord of the plate at span location $b - \frac{\Delta y}{2}$ for the case given in Fig. 4.7 for different number of panels. $M_\infty = 2.5$, $\alpha = 2^o$, $AR = 1.0$

In Fig. 4.8, the variation of the intensity of vorticity γ along the chord for the above case given in Fig. 4.7 is shown using different number of panels used for computation. The Mach number is 2.5, angle of attack,α, is 2^o and aspect ratio is 1. For this case, γ is worked out at a station just inboard of the tip of the plate. i.e, $y = b - \frac{\Delta y}{2}$, where b is the semi-span length of the panel. Δy is the span-wise width of the element.

It can be seen that the results converge with the increase in total number of panels.

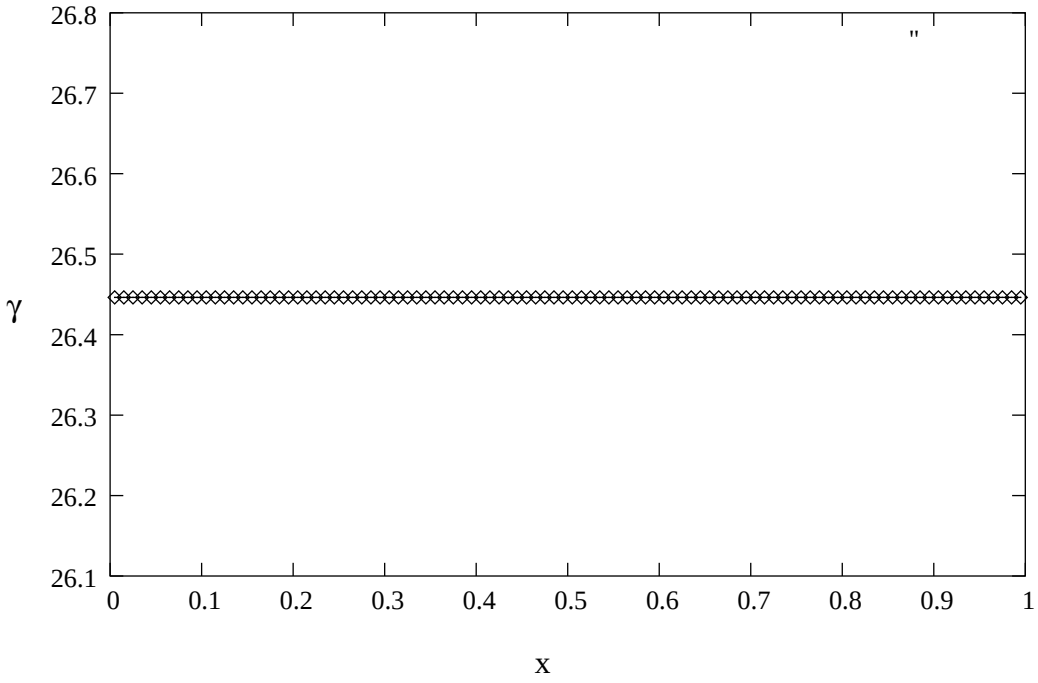

Figure 4.9: Variation of intensity of vorticity along the chord of the plate at at mid-span location for the case given in Fig. 4.7. $M_\infty = 2.5$, $\alpha = 2^o$, $AR = 1.0$

In Fig. 4.9, the variation of γ at the mid-span location is shown. In this case, the flow is supersonic in the region considered. Since the mid-span location is in the region I where flow is two dimensional, γ should remain constant. Two dimensional expression for γ is given by

$$\gamma = \frac{2V_\infty \alpha}{\beta} \tag{4.1}$$

For the values used in Fig. 4.9, the theoritical two dimensional value is given by 26.446. The agreement is seen to be very good.

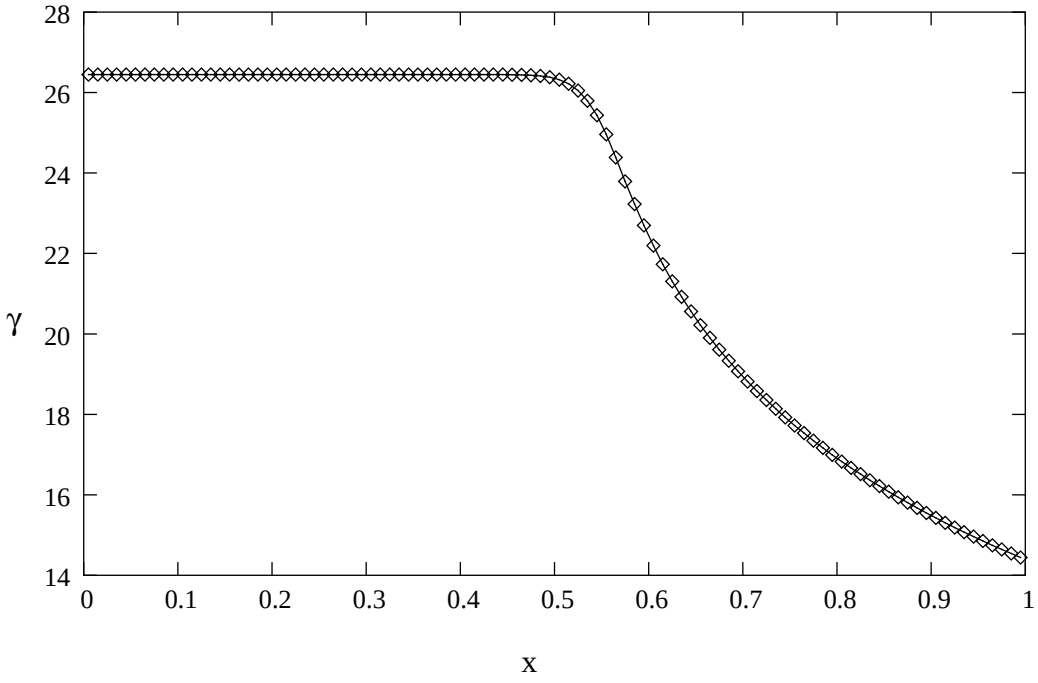

Figure 4.10: Variation of intensity of vorticity along the chord of the plate at at span location $0.75b$ for the case given in Fig. 4.7 . $M_\infty = 2.5$, $\alpha = 2^o$, $AR = 1.0$

In Fig. 4.10, the variation of γ at $y = 0.75b$ location is shown. For this case, when the traverse is made along the chord direction upto $x = 0.57b$, the flow is two dimensional and hence γ does not vary. Beyond $x = 0.57b$, flow is conical resulting in a decrease in value of γ. For this case, trailing edge being supersonic at $x = 1$, γ remains finite.

In Fig. 4.11, the variation of γ at $y = b - \frac{\Delta y}{2}$ location is shown. This is the case considered for the steady convergence. For this case, the chosen span location being in region of conical flow, the value of γ decreases monotonically from leading edge to the trailing edge.

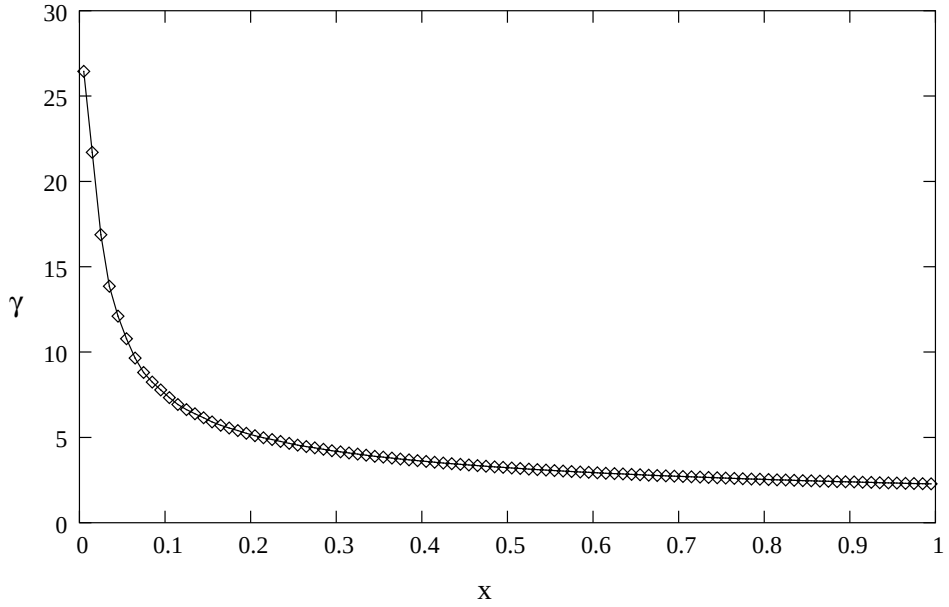

Figure 4.11: Variation of intensity of vorticity along the chord of the plate at at span location $b - \frac{\Delta y}{2}$ for the case given in Fig. 4.7. $M_\infty = 2.5$, $\alpha = 2^o$, $AR = 1.0$

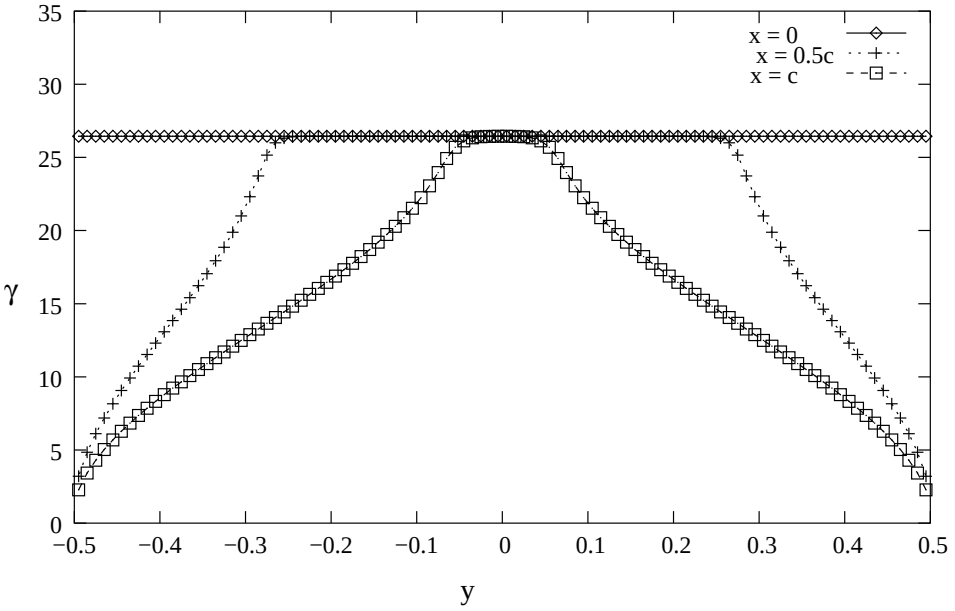

Figure 4.12: Variation of intensity of vorticity along the span of the plate at different chord locations for the case given in Fig. 4.7. $M_\infty = 2.5$, $\alpha = 2^o$, $AR = 1.0$

In Fig. 4.12, the variation of γ versus y at different x locations are shown. For this case, in the interior portion flow being two dimensional, γ remains constant and drops to a value nearly zero in the neighbourhood of the tip of the plate. As x increases, the width of the region I, where flow is two dimensional, decreases. This is clearly seen in Fig. 4.12.

The value of coefficient of normal load,C_N was calculated for this case and found to be 0.0478574. Reference area is the planform are of the plate.

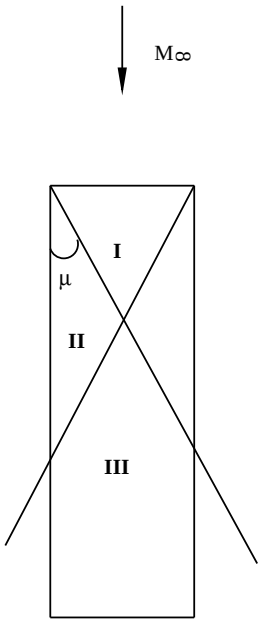

Figure 4.13: Rectangular flat plate wing. $M_\infty = 2.5$,$AR = 0.25$

In Fig. 4.13, the rectangular flat plate with $AR = 0.25$ in supersonic free stream Mach number of 2.5 is shown. For this case, in the region I flow is two dimensional, region II is conical and region III is neither two dimensional nor conical.

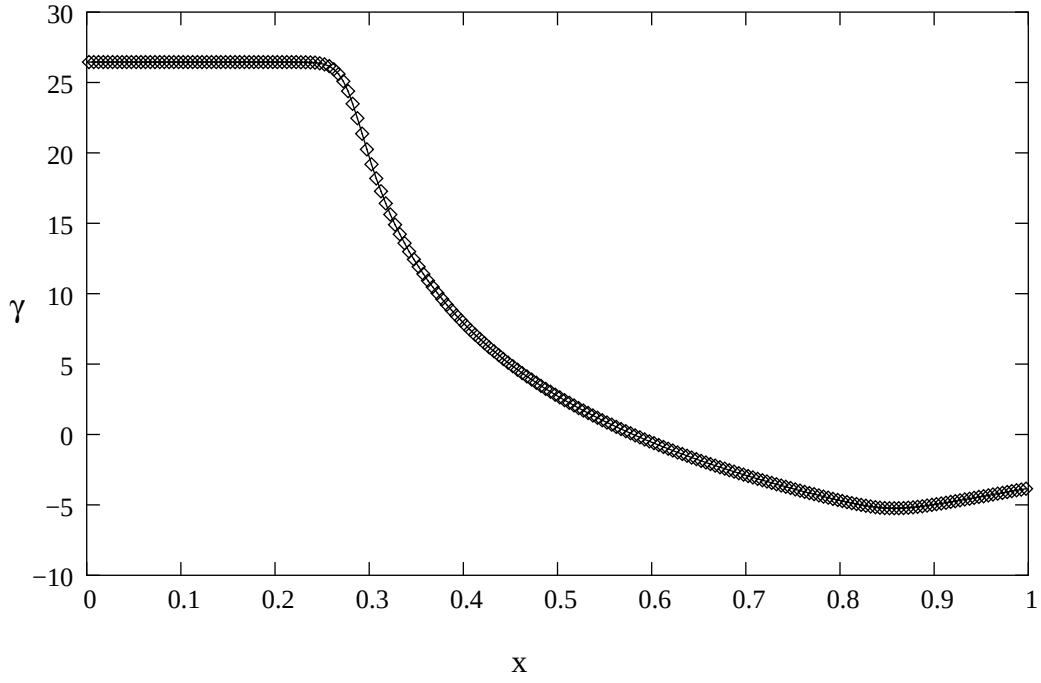

Figure 4.14: Variation of intensity of vorticity along the chord of the plate at at mid-span location for the case given in Fig. 4.13. $M_\infty = 2.5$, $\alpha = 2^o$, $AR = 0.25$

In Fig. 4.14, the variation of γ at the mid-span location is shown. For the case given in Fig. 4.13, since the initial portion of flow being two dimensional, γ remains constant. Beyond that it starts decreasing and becomes negative. Near the trailing edge of the plate, γ starts increasing and becomes closer to value zero. It is in agreement with the known fact that even for supersonic flow, for a fixed span length, as the chord length is increased, the load at the trailing edge should be zero. Hence, theoritically for this case, γ should go to zero. Fig. 4.14.

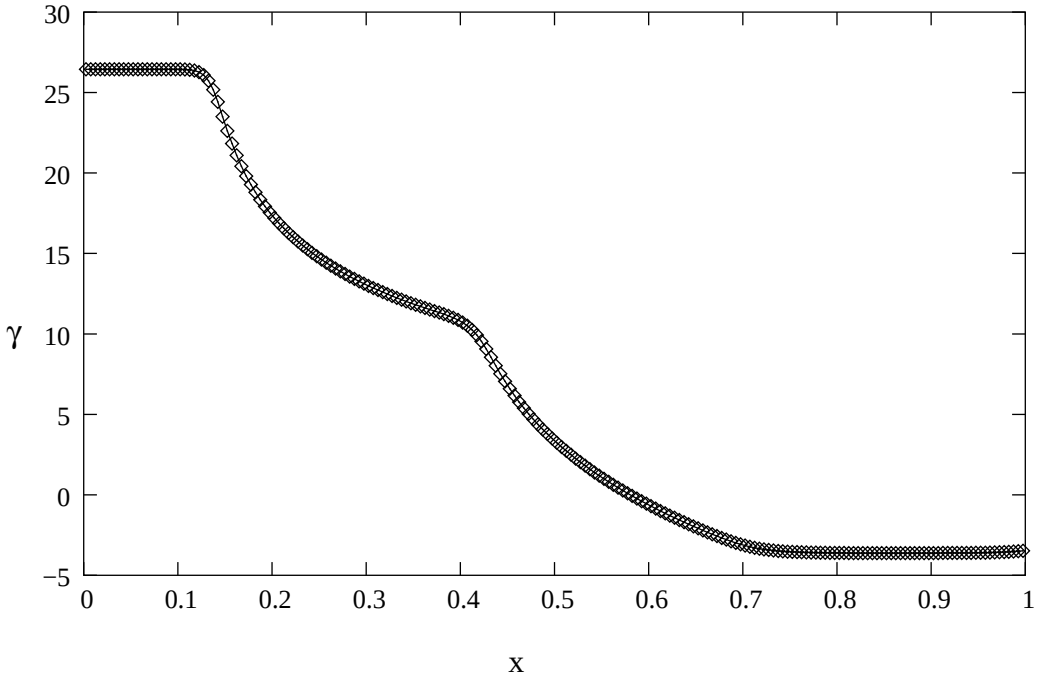

Figure 4.15: Variation of intensity of vorticity along the chord of the plate at at span location $0.75b$ for the case given in Fig. 4.13. $M_\infty = 2.5$, $\alpha = 2^o$, $AR = 0.25$

In Fig. 4.15, the variation of γ at $y = 0.75b$ location is shown. In this case, the flow is two dimensional, then becomes conical. For values of x around 0.4, the flow becomes neither two dimensional nor conical. It can be seen that value of γ is remain constant till the point of intersection of first Mach cone, decreases till the intersection of second Mach cone, decreases initially after the second Mach cone and becomes constant.

In Fig. 4.16, the variation of γ at $y = b - \frac{\Delta y}{2}$ location is shown. In this case, the flow is conical till the intersection of Mach cone and neither conical nor supersonic after that. Hence the value of γ is expected to decrease from the leading edge till the intersection of Mach cone, decrease and become constant after that. In Fig. 4.16 this trend can be clearly seen.

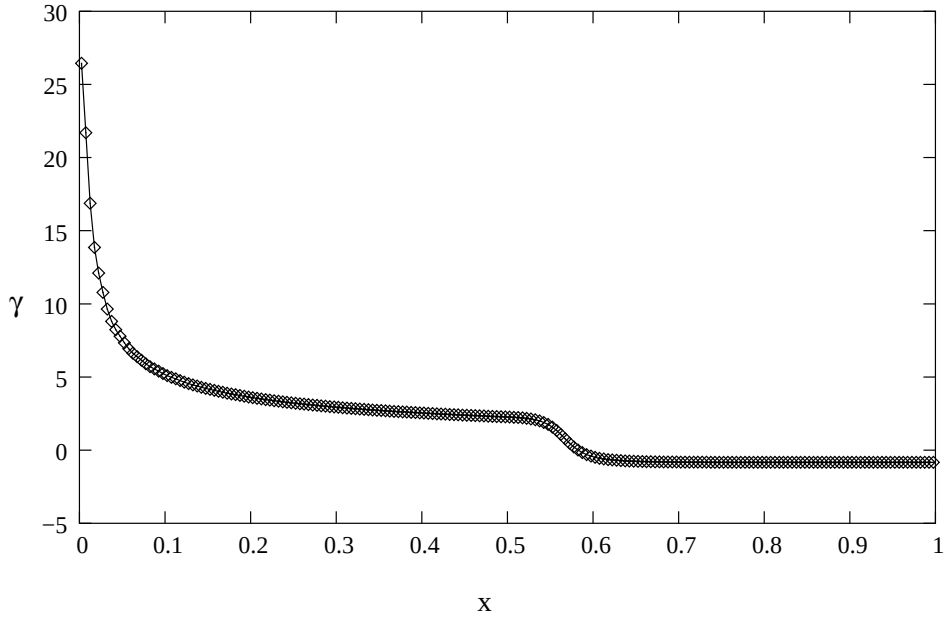

Figure 4.16: Variation of intensity of vorticity along the chord of the plate at at span location $b - \frac{\Delta y}{2}$ for the case given in Fig. 4.13. $M_\infty = 2.5$, $\alpha = 2^o$, $AR = 0.25$

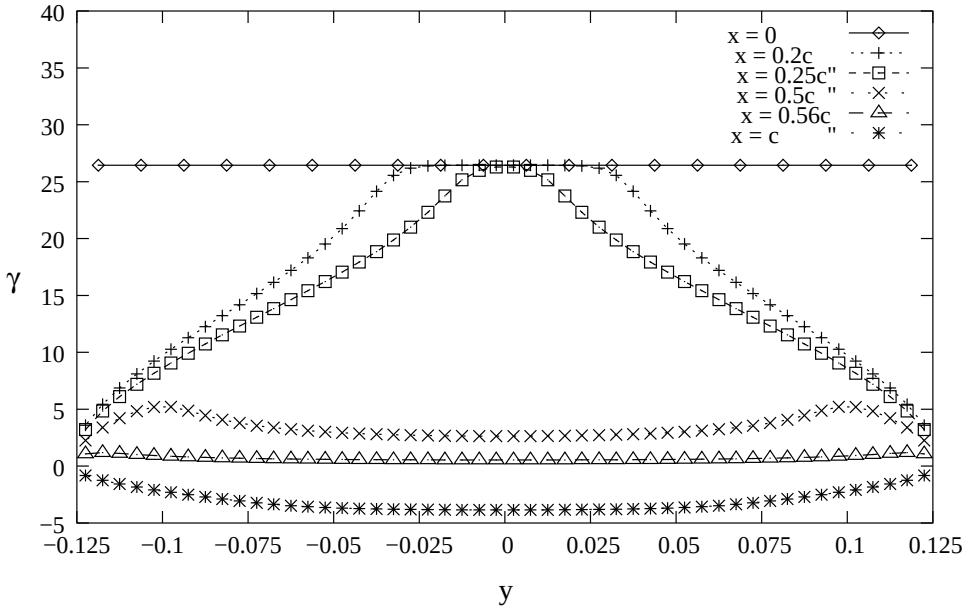

Figure 4.17: Variation of intensity of vorticity along the span of the plate at at different span locations for the case given in Fig. 4.13. $M_\infty = 2.5$, $\alpha = 2^o$, $AR = 0.25$

In Fig. 4.17, the variation of γ versus y at different x locations are shown. For this case, at $x = 0$ since all the points along the span direction lie in the two dimensional region, there is no variation in the value of γ. For $x = 0.25c$, only over a small length in the neighbourhood of $y = 0$, flow is two dimensional and γ starts decreasing as one moves towards the tip of the wing. It is interesting that for $x = 0.56c$, for all points along the span direction $\gamma = 0$.

The value of coefficient of normal load,C_N was calculated for this case and is found to be 0.0150287.

According to Liepmann and Roshko. [5], the coefficient of lift for a finite aspect ratio flat plate is given by

$$C_L = C_{L_0}\left(1 - \frac{1}{2AR\sqrt{M_\infty^2 - 1}}\right) \tag{4.2}$$

where C_{L_0} is the lift coefficient for a two dimensional plate and is given by

$$C_{L_0} = \frac{4\alpha}{\sqrt{M_\infty^2 - 1}} \tag{4.3}$$

where α is the angle of attack and M_∞ is the freestream Mach number. Hence,

$$C_L = \frac{4\alpha}{\sqrt{M_\infty^2 - 1}}\left(1 - \frac{1}{2AR\sqrt{M_\infty^2 - 1}}\right) \tag{4.4}$$

It should be noted that the above equation C_L is restricted to those finite aspect ratio rectangular flat plates in which the Mach cone from the tips of the plate do not intersect within the chord length of the plate. For small angles of attack, $C_L = C_N$. In table. 4.1, a comparison of the normal force coefficient obtained from the present method and that obtained from Eqn. 4.4 is shown.

Table 4.1: Comparison of normal force coefficient for a rectangular flat plate obtained from the present method and that given in Liepmann.et.al. [5] for different aspect ratio. $M_\infty = 2.5$, $\alpha = 2^o$

AR	C_N(present)	C_N(Eqn. 4.4)
0.1	0.00579	-
0.25	0.01503	-
0.5	0.03478	-
1	0.04786	0.04764
4	0.05782	0.05761
7	0.05919	0.05904
10	0.05971	0.05961

In the table. 4.1, for values of AR from 0.1 to 0.5, the Mach cones from the two ends of the leading edge intersect on the plate and hence the expresion given by Eqn. 4.4 cannot be used. It is clearly seen that for AR 1 to 10, the agreement between present values and ones obtained from the Eqn. 4.4 are very good.

It is interesting to compare the results obtained using linear theory and exact theory. In Appendix. D, comparison between linear theory and exact theory applied to a two dimensional flat plate is shown. It can be seen that values of normal force good show good agreement even at angle of attack 10^o.

4.3 Combined, internal and External flow past cylindrical duct

In this section, supersonic flow past cylindrical ducts are studied. For this case, the radius of duct is fixed to 1. Since vorticity distribution is i used both the internal and external flow are obtained simultaneously. Results were obtained for different lengths of the duct. Result are obtained also for different angles of attack.

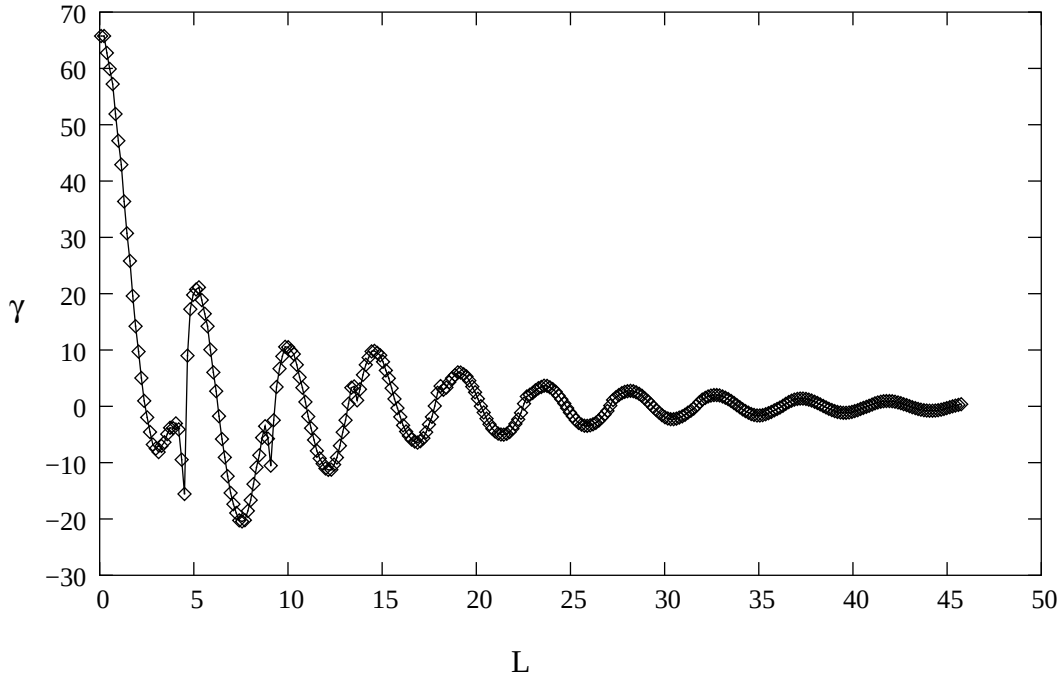

Figure 4.18: Variation of intensity of vorticity along the length of the duct at $\theta = 0$ plane. $M_\infty = 2.5$, $\alpha = 2^o$

In Fig. 4.18, the variation of γ is shown at $\theta = 0$ plane. It can been that it is oscillatory. Mainly, oscillation is due to internal flow. It amy be mentioned as seen in Fig. 4.3 and Fig. 4.2, that the intensity of vorticity and other quantities exhibited oscillations for internal flow. Since external flow alone cannot induce oscillations, the combined flow must also be oscillatory and this is in accordance with the result obtained from internal flow through the cylinder. As the length of the duct is increased, γ tends to zero, which is in agreement with the intuitive understanding of the flow field. For the present case, inspite of the freestream Mach number being supersonic, angle of attack being very small, cross flow Mach number is 0.0873. Hence the behaviour of the cross flow is subsonic. Hence as the length of the duct is increased, at $x = L$, γ should be equal to zero.

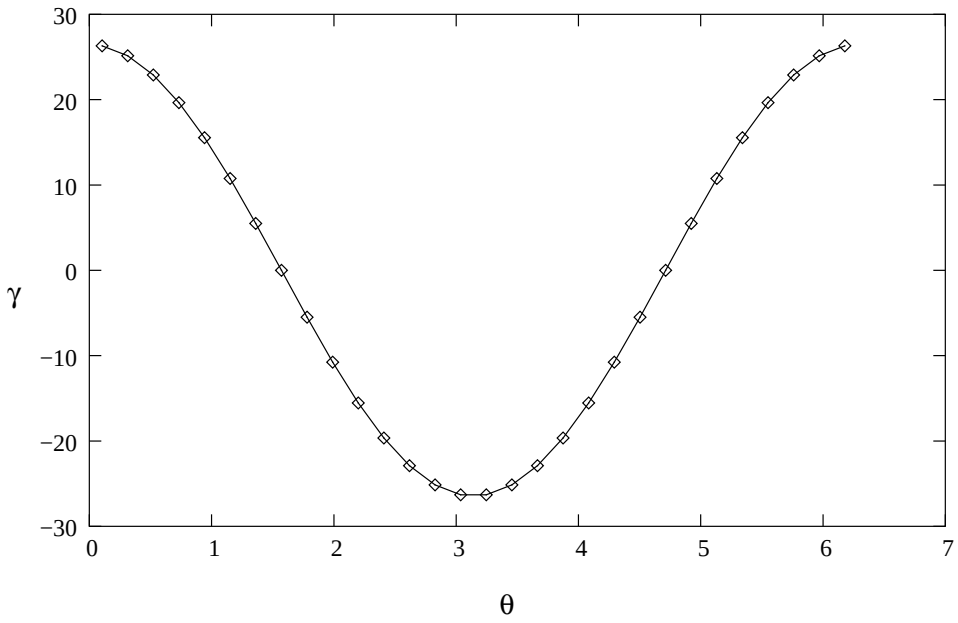

Figure 4.19: Variation of intensity of vorticity along the circumference of the duct at $x = 0$. $M_\infty = 2.5$, $\alpha = 2^o$

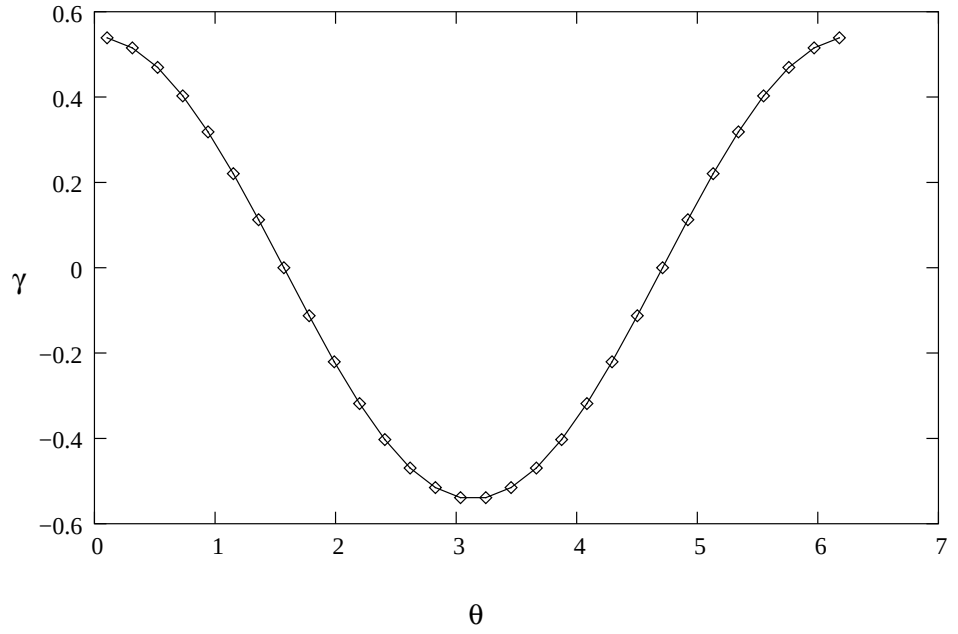

Figure 4.20: Variation of intensity of vorticity along the circumference of the duct at $x = 20$. $M_\infty = 2.5$, $\alpha = 2^o$

In Fig. 4.19 and Fig. 4.20, the variation of γ versus θ is shown respectively at $x = 0$ and $x = 20$. It can be seen that it is a cosine curve and the outcome of calculation confirms the existing similarity for γ in the circumferential direction.

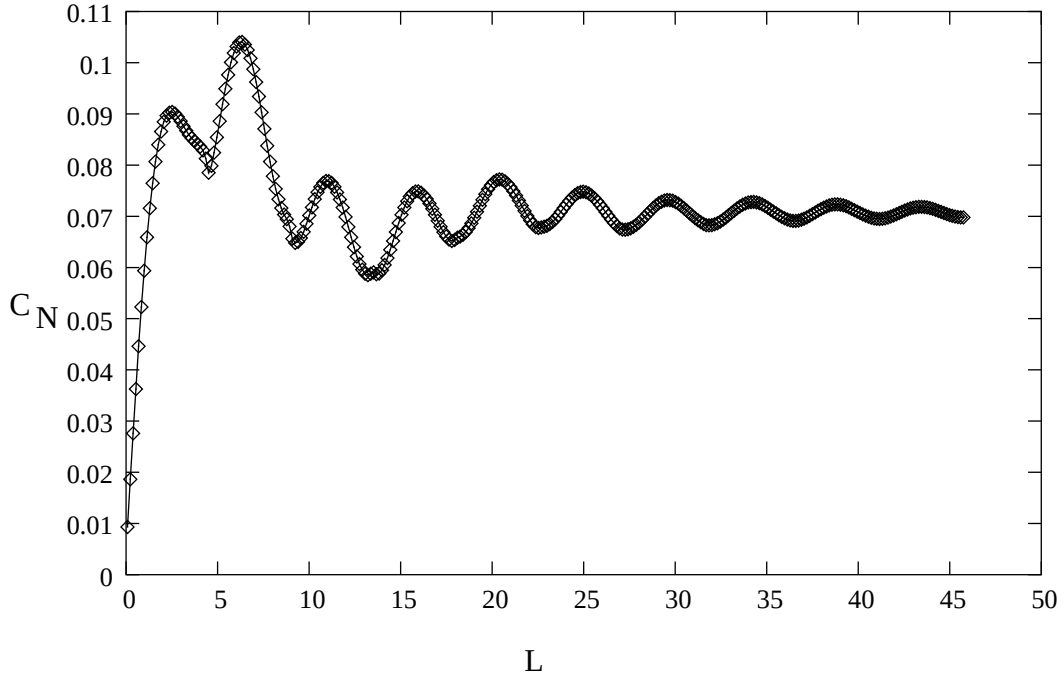

Figure 4.21: Variation of normal force coefficient with the length of the duct. $M_\infty = 2.5$, $\alpha = 2^o$

In Fig. 4.21, the variation of C_N versus L. It can be seen that the value of C_N increases initially and then starts oscillating. It can also be seen that the oscillation dies down as L increases and the value of C_N becomes constant as it should. However, the value obtained is exactly half the value obtained using subsonic theory. Since the normal load depends only on cross flow, the values obtained using purely supersonic theory should nearly be same as one obtained using subsonic theory.

Chapter 5

Conclusions

It is seen that the results obtained in the present work for the internal flow are in very good agreement with the ones obtained using FLUENT even for large value of duct length at small angles of attack. At large angles of attack, the present resutls and the ones obtained using FLUENT start deviating for larger values of length of the duct. The combined, internal and external flow past the duct was studied using distribution of vorticity and the for this case validation was carried out considering the case of a flat plate in uniform supersonic flow. For this case, present results are in good agreement with the ones in the literature. However, the results obtained for the combined flow past the cylindrical duct is not conclusive due to the following reason. The present results did not agree with the ones got using FLUENT. However, since the result obtained using FLUENT did not the converge to the desired accuracy, the results are not presented.

Appendix A

Self induced velocity of source panel

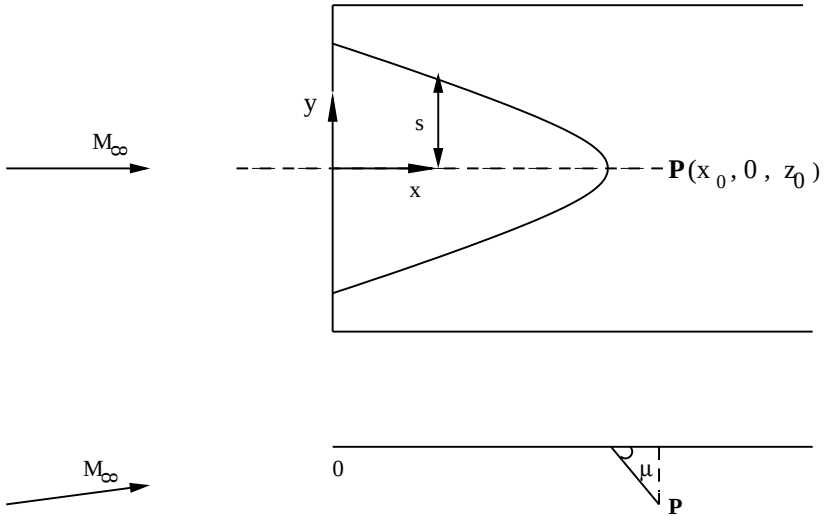

Figure A.1: Panel with uniform distribution of source

In the Fig. A.1, a panel with uniform distribution of source of intensity q is shown. The panel is situated in $z = 0$ plane. $P(x_0, 0, z_0)$ is a point below the panel. The intersection of the upstream Mach cone of P and the panel is shown.

The equation of the curve of intersection of the upstream Mach cone and the panel is given by

$$s = \pm \left[\frac{(x-x_0)^2}{\beta^2} - {z_0}^2 \right]^{\frac{1}{2}} \tag{A.1}$$

Now the potential at point P is given by Eqn. 2.1. Simplifying it for the present case,

$$\phi_p = -\frac{q}{2\pi} \int_0^{x_0+\beta z_0} \int_{-s}^{s} \frac{1}{[(x-x_0)^2 - \beta^2(y^2+(z_0)^2]^{\frac{1}{2}}} dxdy \tag{A.2}$$

Now,

$$I = \int_{-s}^{s} \frac{1}{[(x-x_0)^2 - \beta^2(y^2+z_0)^2]^{\frac{1}{2}}} dy = \frac{1}{\beta} \int_{-s}^{s} \frac{1}{\left[\frac{(x-x_0)^2}{\beta^2} - y^2 - {z_0}^2\right]^{\frac{1}{2}}} dy \tag{A.3}$$

From, Eqn. A.1 we note that $\frac{(x-x_0)^2}{\beta^2} - {z_0}^2 = s^2$. Therefore,

$$I = \frac{1}{\beta} \int_{-s}^{s} \frac{dy}{(s^2-y^2)^{\frac{1}{2}}} = \frac{\pi}{\beta} \tag{A.4}$$

Hence Eqn. A.2 reduces to

$$\phi_p = -\frac{q}{2\pi} \times \frac{\pi}{\beta} \int_0^{x_0+\beta z_0} dx = -\frac{q}{2\beta}(x_0+\beta z_0) \tag{A.5}$$

Hence from Eqn. 2.6 self induced velocity, i.e.w at $z_0 = 0$ is given by,

$$w^* = \left.\frac{\partial \phi}{\partial z_0}\right|_{z_0=0} = -\frac{q}{2} \tag{A.6}$$

Appendix B

Finite Part of a Divergent Integral

Let us consider the integral

$$I(\varepsilon) = \int_{a+\varepsilon}^{b} \frac{f(x)}{(x-a)^{\frac{3}{2}}}\,dx \tag{B.1}$$

where $f'(x)$ is assumed to exist and to be bounded for $a \leq x \leq b$. If $\varepsilon > 0$, then this integral exists, but if $\varepsilon = 0$, then the integral is divergent, and no meaning can be assigned to $I(0)$. The integral $I(\varepsilon)$ can be written as

$$\begin{aligned} I(\varepsilon) &= \int_{a+\varepsilon}^{b} \frac{f(x)-f(a)}{(x-a)^{\frac{3}{2}}}\,dx + f(a)\int_{a+\varepsilon}^{b} \frac{dx}{(x-a)^{\frac{3}{2}}} \\ &= \int_{a+\varepsilon}^{b} \frac{f(x)-f(a)}{(x-a)^{\frac{3}{2}}}\,dx + f(a)\left(\frac{2}{\varepsilon^{\frac{1}{2}}} - \frac{2}{(b-a)^{\frac{1}{2}}}\right) \end{aligned} \tag{B.2}$$

As $\varepsilon \to 0$, the first integral exists as an ordinary improper integral, and the last term exists, so Eqn.B.2 can be written as

$$I(\varepsilon) = \int_{a}^{b} \frac{f(x)-f(a)}{(x-a)^{\frac{3}{2}}}\,dx + \frac{2f(a)}{\varepsilon^{\frac{1}{2}}} - \frac{2f(a)}{(b-a)^{\frac{1}{2}}} - \int_{a}^{a+\varepsilon} \frac{f(x)-f(a)}{(x-a)^{\frac{3}{2}}}\,dx \tag{B.3}$$

If the first two terms are denoted by $*I$, this shows that

$$I(\varepsilon) = *I + \frac{A}{\varepsilon^{\frac{1}{2}}} + o(\varepsilon) \tag{B.4}$$

where $o(\varepsilon)$ denotes a function that tends to zero with ε, whence

$$*I = \lim_{\varepsilon \to 0} \left(I(\varepsilon) - \frac{A}{\varepsilon^{\frac{1}{2}}} \right) \tag{B.5}$$

Hadamard(1923) called this unique limit, $*I$, the finite part of $I(0)$, and it is denoted by a star placed in front of the integral, thus

$$* \int_a^b \frac{f(x)}{(x-a)^{\frac{3}{2}}} dx = \int_a^b \frac{f(x) - f(a)}{(x-a)^{\frac{3}{2}}} dx - \frac{2f(a)}{(b-a)^{\frac{1}{2}}} - \tag{B.6}$$

Appendix C

Self induced velocity of vortex panel

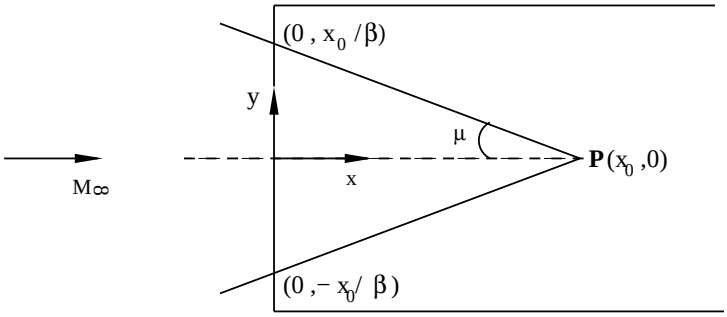

Figure C.1: Vortex panel with uniform distribution of vorticity

In the Fig. C.1, a vortex panel with uniform distribution of vorticity of intensity γ, is shown. $P(x_0, 0)$ is a point on the panel. The upstream Mach cone from point P is shown. The Mach angle μ is given by $tan^{-1}(\frac{1}{\beta})$, where β is given by $\sqrt{M_\infty{}^2 - 1}$. Hence the equation of the curve of intersecion of the upstream cone and the panel is given by

$$x = x_0 - \beta|y| \tag{C.1}$$

Now the coordinates of points of intersection of Mach cone and the leading edge of the panel can be obtained as $(0, \frac{-x_0}{\beta}$ and $(0, \frac{x_0}{\beta})$. Using the equation for the w component

of velocity as given in Robinson. [1] and simplifying it for the present case we get

$$\begin{aligned} w^* &= -\frac{\beta^2\gamma}{2\pi}\int_{\frac{-x_0}{\beta}}^{\frac{x_0}{\beta}}\int_0^{x_0-\beta|y|}\frac{(x_0-x)}{[(x_0-x)^2-\beta^2y^2]^{\frac{3}{2}}}\,dxdy \\ &= -\frac{\beta^2\gamma}{2\pi}\int_{\frac{-x_0}{\beta}}^{0}\int_0^{x_0+\beta y}\frac{(x_0-x)}{[(x_0-x)^2-\beta^2y^2]^{\frac{3}{2}}}\,dxdy - \frac{\beta^2\gamma}{2\pi}\int_0^{\frac{x_0}{\beta}}\int_0^{x_0-\beta y}\frac{(x_0-x)}{[(x_0-x)^2-\beta^2y^2]^{\frac{3}{2}}}\,dxdy \end{aligned}$$

Due to symmetry, the equation reduces to

$$w^* = -\frac{2\beta^2\gamma}{2\pi}\int_0^{\frac{x_0}{\beta}}\int_0^{x_0-\beta y}\frac{(x_0-x)}{[(x_0-x)^2-\beta^2y^2]^{\frac{3}{2}}}\,dxdy \tag{C.2}$$

Taking the finite part of the integral and noting that sign of finite part does not follow the sign of the integrand, refer Robinson. [1].

$$*\int_0^{x_0-\beta y}\frac{(x_0-x)}{[(x_0-x)^2-\beta^2y^2]^{\frac{3}{2}}}\,dx = \frac{1}{[{x_0}^2-\beta^2y^2]^{\frac{1}{2}}} \tag{C.3}$$

Substituting this equation in Eqn. C.2, we get

$$\begin{aligned} w^* &= -\frac{\beta^2\gamma}{\pi}\int_0^{\frac{x_0}{\beta}}\frac{1}{[{x_0}^2-\beta^2y^2]^{\frac{1}{2}}}\,dy \\ &= -\frac{\beta^2\gamma}{\pi}\left[sin^{-1}(\frac{y\beta}{x_0})\Big|_0^{\frac{x_0}{\beta}}\right] \\ &= -\frac{\gamma\beta}{2} \end{aligned} \tag{C.4}$$

Appendix D

Limitation of Linear theory

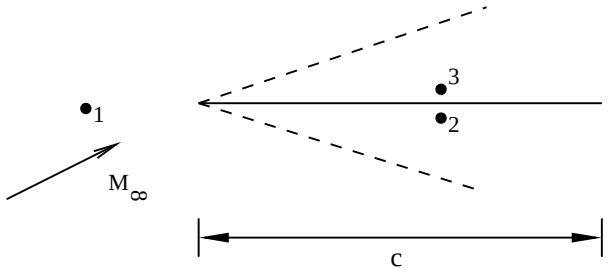

Figure D.1: 2D plate in supersonic flow

In Fig. D.1, a two dimensional plate in supersonic flow is shown. The coefficient of normal force, C_N was computed using linear theory and shock-expansion theory, which is exact theory, for different angles of attack and compared.
According to linear theory, coefficient of normal force is given by

$$C_N = \frac{4\alpha}{\sqrt{{M_\infty}^2 - 1}} \tag{D.1}$$

According to shock-expansion theory, the pressure at region 2 is given by shock theory

$$\frac{P_2}{P_1} = 1 + \frac{2\gamma}{\gamma+1}\left({M_1}^2 \sin^2\beta - 1\right) \tag{D.2}$$

where β is obtained from

$$\tan\theta = 2\cot\beta\left[\frac{M_1^2\sin^2\beta - 1}{M_1^2(\gamma+\cos 2\beta)+2}\right] \tag{D.3}$$

where θ is the angle of attack.

The pressure at region 3 can be obtained using expansion wave theory.

$$\frac{P_3}{P_1} = \left[\frac{1+\frac{\gamma-1}{2}M_1^2}{1+\frac{\gamma-1}{2}M_3^2}\right]^{\frac{\gamma}{\gamma-1}} \tag{D.4}$$

where M_3 can be obtained from Eqn. D.6. $\gamma(M_3)$ is obtained from

$$\gamma(M_3) = \gamma(M_1) + \theta \tag{D.5}$$

where θ is the angle of attack and $\gamma(M_1)$ is obtained from Eqn. D.6.

$$\gamma(M) = \sqrt{\frac{\gamma+1}{\gamma-1}}\tan^{-1}\sqrt{\frac{\gamma-1}{\gamma+1}(M^2-1)} - \tan^{-1}\sqrt{M^2-1} \tag{D.6}$$

Now the coefficient of normal load is given by

$$C_N = \frac{2}{\gamma M_1^2}\left[\frac{P_3 - P_2}{P_1}\right] \tag{D.7}$$

Tabulated below are the values of coefficient of normal load at various angles of attack using both the theories.

Table D.1: Comparison of C_N at various angles of attack

α	$C_N(linear)$	$C_N(actual)$
2	0.0609	0.0610
4	0.1219	0.1225
6	0.1828	0.1849
8	0.2438	0.2488
10	0.3047	0.3144

It can be seen that the agreement in the values of C_N is good even for angle of attack of 10^o.

Bibliography

[1] Robinson A. Linearized theory of steady supersonic flow. *Quarterly Journal of Mechanics and Applied Mathematics*, pages 408–432, 1948.

[2] Burkhalter J.E. Grid fins for missile applications in supersonic flow. *AIAA Paper 1996 - 0194*, January 1996.

[3] Burkhalter J.E and H.M .Frank. Grid fin aerodynamics for missile applications in subsonic flow. *Journal of Spacecraft and Rockets*, 33(1):38–44, 1996.

[4] John.D.Anderson. Jr. *Modern compressible flow, second edition*. McGraw-Hill Publishing company, 1990.

[5] H. W. Liepmann and A.Roshko. *Elements of Gas Dynamics*. John Wiley & Sons.Inc., 1956.

[6] Miranda L.R., Elliott R.D., and Baker W.M. A generalized vortex lattice method for subsonic and supersonic flow applications. *NASA Contractor Report 2865*, 1977.

[7] Ward G. N. *Linearized Theory of Steady High-Speed Flow*. Cambridge University Press, 1955.

[8] Brooks R.A and Burkhalter J.E. Experimental and analytical analysis of grid fin configurations. *Journal of Aircraft*, 26(9):885–887, January 1993.

[9] Prabhu Ramachandran.and S. C. Rajan. and S. Santhakumar. Obtaining engineering estimates of aerodynamic forces on air-breathing slender bodies. *6th Annual CFD Symposium. Aeronautical Society of India*, August 2003.

[10] Prabhu Ramachandran., S. C. Rajan., and S. Santhakumar. Engineering estimates of normal loads on slender air-breathing bodies. *Journal of Spacecraft and Rockets*, 41(3), May-June 2004(tentative).

[11] S. Santhakumar, S. C. Rajan, and B. Venkata Subbaiah. Aerodynamic design and analysis of grid fins. *interim report on IIT reference No: RB/02-03/ASE/001/DRDL/SSAN*, July 2003.